



# Revised production cross-section of $\gamma$ -rays in p-p collisions with LHC data for the study of TeV $\gamma$ -ray astronomy

H. Sato, T. Shibata, R. Yamazaki

*Department of Physics and Mathematics, Aoyama-Gakuin University,  
Chuo-ku Fuchinobe 5-10-1, Kanagawa 252-5258, Japan*

---

## Abstract

We present the production cross-section of  $\gamma$ -rays based on data of p-p collisions at the Large Hadron Collider (LHC), revising the previous semi-empirical formula mainly for 1) the inelastic cross-section in p-p collisions,  $\sigma_{pp}(E_0)$ , and 2) the inclusive  $\gamma$ -ray spectrum in the forward region,  $\sigma_{pp \rightarrow \gamma}(E_0, E_\gamma)$ . We find that the previous cross-section gives a significantly softer spectrum than found in the data of LHC. In this paper, we focus our interest mainly upon the LHC forward (LHCf) experiment, giving  $\gamma$ -ray spectra in the very forward region with the pseudo-rapidity  $\eta^* \gtrsim 8.8$  in the center of mass system (CMS), which have not been reported so far. We also give the pseudo-rapidity distribution of charged hadrons with  $-3 \leq \eta^* \leq 3$  obtained by ALICE and TOTEM experiments, both with LHC. We find that the revised cross-section reproduces quite well the accelerator data over the wide energy range from GeV to 30 PeV for projectile protons, corresponding approximately to 100 MeV to 3 PeV for secondary  $\gamma$ -rays. The production cross-section of  $\gamma$ -rays produced in the forward region is essential for the study of  $\gamma$ -ray astronomy, while not important are those produced in the central region in CMS, and of much less importance in the backward. We discuss also the average transverse momentum of  $\gamma$ -rays,  $\bar{p}_t$ , and the average inelasticity transferred to  $\gamma$ -rays,  $\bar{k}_\gamma^*$ , obtaining that the former increases very slowly with  $\bar{p}_t = 100 \sim 220$  MeV/c for  $E_0 = 1$  GeV  $\sim 26$  PeV, and the latter is almost independent of  $E_0$ , with  $\bar{k}_\gamma^* \approx 1/6$ , while we can not exclude the possibility of a small increase of  $\bar{k}_\gamma^*$ .

*Keywords:* cosmic-ray; gamma-rays; LHC; cross-section

---

## 1. Introduction.

The high energy  $\gamma$ -ray observations open a new window not only for the astronomy, but also for the particle physics, cosmology, which must bring us critical information and hints for the understanding of current questions such as nature of the dark matter, mechanism of the  $\gamma$ -ray burst, origin of the highest

cosmic-ray (CR), and so forth. In recent years, remarkably developed are techniques in both on-board and ground-based telescopes, *Fermi*, H.E.S.S., MAGIC, VERITAS, which have reported exciting results for the sky-map of GeV-TeV  $\gamma$ -rays in space, still working continuously, see [2] for review.

A new program called CTA (Cherenkov Telescope Array) is further progressing in the form of the international collaboration consisting of many scientists from Europe, USA and Japan [28]. It covers very wide energy range of  $\gamma$ -rays with several tens GeV to more than 10 TeV with much higher sensitivity than ever achieved, the full operation of which is scheduled around 2020. If the CTA program is operated as scheduled, we expect to detect TeV  $\gamma$ -ray sources more than thousands, comparable with those currently observed in GeV region, which must bring us surely new aspects for the understanding of the universe.

Under these situations, it is quite desirable to have a reliable production cross-section of hadron-induced  $\gamma$ -rays with TeV energy or more, while those of electron-induced ones are, needless to say, well established on the basis of QED. Stecker [3] presented the production cross-section of  $\pi^0$ ,  $\sigma_{pp \rightarrow \pi^0}(E_0, E_{\pi^0})$  with  $E_{\pi^0} \lesssim 100$  GeV ( $E_0 \lesssim 1$  TeV) in the form of very useful parameterizations in 1973, and later one of the authors (T. S.) revised it in the previous paper [1] (hereafter Paper I), applicable for the higher energy region  $E_0 \gtrsim 1$  TeV. Nevertheless, the reliability is not always satisfactory, particularly in the forward region for  $E_\gamma \gtrsim 1$  TeV ( $E_0 \gtrsim 10$  TeV) because of the limitation in the accelerator data, having no data on the energy spectra in the forward region, while Chacaltaya emulsion chamber (EC) group [20, 33] have given them using CR-beams, but poor in data quality.

Fortunately, the LHC experiment started the operations in early 2010, among which the LHCf group measured  $\gamma$ -ray spectra in the very forward region with the pseudo-rapidity  $\eta^* \gtrsim 8.8$  in the CMS [4]. The principal purpose of the LHCf is to find the best simulation code in hadron-interaction models, which plays a key role in the study of the extensive air shower (EAS) phenomena induced by the ultra-high energy CRs, affecting directly the estimation of the primary CR energy as well as its composition. While none of models currently available reproduce satisfactorily the LHCf data according to their preliminary studies [4], they will report a revised model soon based on further analyses as well as on coming data at  $\sqrt{s} = 14$  TeV, the run of which is scheduled in 2014.

Alternatively, the LHCf data also give us crucial information for the study of hadron-induced  $\gamma$ -rays in galactic environments, both interstellar medium (ISM) and the source of CRs, typically the supernova remnant (SNR). Particularly interesting is the production cross-section of  $\gamma$ -rays with 100 TeV or more in the laboratory system (LS), corresponding to the knee energy around PeV. We expect that the knee problem in close connection with the acceleration limit of CRs in the SNR may be solved by the CTA program through the observations of ultra-high energy  $\gamma$ -rays with  $E_\gamma \gtrsim 100$  TeV, possibly much more clearly than those of hadronic components. Note that it is still not cleared albeit so many years have passed since the discovery of the knee [30]. This is mainly due to the difficulty in observing the latter components around the knee energy by both direct (balloon and/or satellite) and the indirect (EAS) methods, which have

Table 1: Numerical values of  $[\sigma_0, \epsilon_0, \kappa]$  appearing in Eqs. (1) and (2) for three cases of target mass,  $1 \leq A_T \leq 4$ ,  $4 < A_T \leq 38$ , and  $38 \leq A_T$ , where  $\sigma_0$  is in units of millibarn (mb), and  $\epsilon_0$  in GeV.

	$1 \leq A_T \leq 4$	$4 < A_T \leq 38$	$38 \leq A_T$
$\sigma_0$ :	20.0	22.3	18.5
$\epsilon_0$ :	0.93	0.92	0.92
$\kappa$ :	2.23	2.40	2.40

inevitable weaknesses in statistics for the former, and in the uncertainty of the composition for the latter.

Now the accelerator data on  $\sigma_{pp \rightarrow \gamma}(E_0, E_\gamma)$  being available over extremely wide energy ranges,  $E_0 = 1 \text{ GeV} \sim 30 \text{ PeV}$ , it is an easy task to find empirically the cross-section by *interpolating* them without asking for complicated models in the meson production. While many phenomenological models with QCD have been applied for the current simulation codes [29], one should keep in mind the fact that even the inelastic collision cross-section based on QCD,  $\sigma_{pp}(E_0)$ , is not yet definitely established, and much less successful are those for the multiple meson production,  $\sigma_{pp \rightarrow \pi}(E_0, E_\pi)$ . In the present paper, we give  $\sigma_{pp \rightarrow \gamma}(E_0, E_\gamma)$  with simple parameterization based on the experimental data with LHC, revising slightly the previous one, which will be quite useful for the study of future  $\gamma$ -ray astronomy even around 100 TeV or more.

## 2. Cross-sections

### 2.1. Inelastic collision cross-section

In Paper I, we gave the empirical formula for the inelastic cross-section,  $\sigma_{pp}(E_0)$ , in p-p collision which covers the wide energy range from the threshold energy of pion production ( $\sqrt{s} \approx 2 \text{ GeV}$ ) to the FNAL energy ( $\sqrt{s} = 1.8 \text{ TeV}$ ). Now we have the LHC data (ATLAS[5], ALICE[23], TOTEM[24]) on  $\sigma_{pp}$  at  $\sqrt{s} = 7 \text{ TeV}$ . The LHC energy currently available corresponds to approximately 26 PeV proton in the LS, high enough even for 100 TeV  $\gamma$ -ray astronomy.

Based on the LHC data, we assume a following empirical form for  $\sigma_{pp}$ ,

$$\sigma_{pp}(E_0) = \Sigma_0(E_0) \left[ 1 + \sqrt[8]{s/s_0} \right], \quad (1)$$

with 
$$\Sigma_0(E_0) = \sigma_0 (c/v)^\kappa \left( 1 - e^{-E_0/\epsilon_0} \right), \quad (2)$$

where  $E_0$  and  $v$  are the kinetic energy and velocity of the projectile proton in LS respectively,  $\sqrt{s_0} = 156 \text{ GeV}$ , and see the first column ( $1 \leq A_T \leq 4$ ) of Table 1 for  $\sigma_0$ ,  $\epsilon_0$ , and  $\kappa$ . Practically,  $\Sigma_0 \approx \sigma_0$  for  $E_0 \gtrsim 10 \text{ GeV}$ .

In Fig. 1, we demonstrate  $\sigma_{pp}$  against  $\sqrt{s}$  including the LHC data, together with the previous empirical curve (dashed curve), and the present one (solid curve) given by Eq. (1) with the numerical values summarized in the first column of Table 1. One sees that the previous one gives significantly over-estimation in the LHC energy region.

For the inelastic collision between nucleus  $i$  and nucleus  $j$ , we give the cross-section based on the optical model [6, 7, 8],

$$\sigma_{ij} = \pi(a_i^2 + a_j^2)[\ln \chi_{ij} + E_1(\chi_{ij}) + \gamma_E], \quad (3)$$

with

$$\chi_{ij} = A_i A_j \frac{\sigma_{NN}}{\pi(a_i^2 + a_j^2)}, \quad (4)$$

where  $A_i$  ( $A_j$ ) is the mass number of the projectile (target) nucleus,  $\gamma_E$  the Euler constant ( $=0.5772$ ),  $E_1(\chi)$  the exponential integral function, and  $a_i$  ( $a_j$ ) is related to the nuclear root-mean-square radius of the nucleus  $i$  ( $j$ ), see [7] for the explicit value of  $a_i$  ( $a_j$ ). Here  $\sigma_{NN}$  is given by Eq. (1), but numerical values of the parameters appearing there depend slightly on the target nucleus  $A_T$  as presented in Table 1.

## 2.2. Production cross-section of $\gamma$ -rays

Now in the following discussions, we use the natural units with  $c = 1$  (the speed of light) unless otherwise mentioned specifically, and the asterisk attached to variables denotes those in the CMS, or else those in the LS.

In Paper I, we assumed that the distributions of the energy and transverse momentum in the multiple meson production are both given by the exponential function,  $\exp[-(E_\gamma^*/T_0 + p_t/p_0)]$  ( $E_\gamma^*$ :  $\gamma$ -ray energy,  $p_t$ : its transverse momentum), which are expected from the fire-ball picture [12]. On the other hand in the QCD picture, the energy distribution is given by the algebraical function,  $(1 - x^*)^m$ , expected from the quark dimensional counting approach [13], where  $x^*$  is the light cone momentum fraction, and  $m$  relates to the number of quarks actively involved in the collision with  $m = 3 \sim 6$  practically.

While both types of the distribution are equivalent in the central region around  $x^* \approx 0$ , we find that the algebraical-type reproduces rather well the LHCf data in the extremely forward region with  $x^* \approx 1$  (see Section 3.3). So in the present paper, we assume a following distribution function for the invariant production cross-section of  $\gamma$ -rays, modifying slightly the functional

Figure 1: Inelastic cross-section  $\sigma_{pp}$  in proton-proton collision as a function of the center of mass energy  $\sqrt{s}$  ([9-11], [5], [23], [24]) with two empirical curves, the present one (solid curve) and the previous one (dashed curve).

form used in Paper I,

$$\frac{1}{\sigma_{\text{pp}}} E_\gamma^* \frac{d^3\sigma}{d^3\mathbf{p}_\gamma^*} = \frac{\bar{N}_\gamma \Theta_{\text{C}}}{4\pi T_{\text{C}}^2} \frac{(1-x^*)^m}{X^*} e^{-p_{\text{t}}/p_0}, \quad (5)$$

with

$$x^* = E_\gamma^*/T_{\text{C}}; \quad T_{\text{C}} = \sqrt{s}/2 = M_{\text{p}}\gamma_{\text{C}}, \quad (6)$$

$$X^* = x^* + \zeta p_{\text{t}}/p_0; \quad p_{\text{t}} = E_\gamma^* \sin \theta^*, \quad (7)$$

where  $\gamma_{\text{C}}$  is the Lorentz factor of CMS against the LS,  $M_{\text{p}}$  the proton mass, and  $\Theta_{\text{C}}$  is the normalization constant.

In Eq. (5), we introduce four parameters,  $[m, \zeta, \bar{N}_\gamma, p_0]$ , where  $m$  corresponds to the *softness* of the energy-spectrum,  $\zeta$  to the correlation strength between  $E_\gamma^*$  and  $p_{\text{t}}$ , and  $\bar{N}_\gamma$  is of course the multiplicity of  $\gamma$ 's, and  $p_0$  links to the average transverse momentum  $\bar{p}_{\text{t}}$  (see Eq. [15]). In the present work, however, we fix the former two, with  $m = 4$  and  $\zeta = 0.02$ , expected from the preparatory calculations [31], and focus our principal work on the determination of the latter two,  $[\bar{N}_\gamma, p_0]$ , (practically  $[\bar{N}_\gamma, \bar{p}_{\text{t}}]$ , see the beginning of Section 3) by the least square method in fitting with the experimental data.

In order to make following discussions easy to understand, we introduce a parameter  $\tau_{\text{C}}$ , corresponding to  $\tau_0$  defined by Paper I,

$$\tau_{\text{C}} = T_{\text{C}}/p_0 = \sqrt{s}/2p_0, \quad (8)$$

and  $\Theta_{\text{C}}$  is given by

$$\frac{1}{\Theta_{\text{C}}} = \int_0^1 \frac{F_0(\tau_\theta^*)}{x^\ell (1-x)^4} d(\cos \theta^*); \quad \tau_\theta^* = \tau_{\text{C}} \sin \theta^*, \quad (9)$$

$$F_\ell(\tau) = \int_0^1 x^\ell (1-x)^4 e^{-\tau x} dx, \quad (\ell = 0, 1). \quad (10)$$

with

In Table 2 we give the explicit forms of  $F_\ell(\tau)$  ( $\ell = 0, 1$ ), together with those of the approximation around  $\tau \approx 0$ , and demonstrate the numerical value of  $\Theta_{\text{C}}$  against  $\tau_{\text{C}}$  for several choices of  $\zeta$  in Fig. 2.

Table 2: Explicit forms of  $F_0(\tau)$  and  $F_1(\tau)$ , and their approximate expressions for  $\tau \approx 0$ .

explicit forms of $F_0(\tau)$ and $F_1(\tau)$	for $\tau \approx 0$
$F_0(\tau) = \frac{1}{\tau} - \frac{4}{\tau^2} + \frac{12}{\tau^3} - \frac{24}{\tau^4} + \frac{24}{\tau^5} \left[ 1 - e^{-\tau} \right]$	$\approx \frac{1}{5} - \frac{\tau}{30} + \frac{\tau^2}{210}$
$F_1(\tau) = \frac{1}{\tau^2} - \frac{8}{\tau^3} + \frac{36}{\tau^4} - \frac{96}{\tau^5} + \frac{120}{\tau^6} \left[ 1 - \left( 1 + \frac{\tau}{5} \right) e^{-\tau} \right]$	$\approx \frac{1}{30} - \frac{\tau}{105} + \frac{\tau^2}{560}$

Figure 2: Normalization constant  $\Theta_C$  against  $\tau_C$  for several choices of  $\zeta$ .

### 2.3. Energy-angular distribution

Eq. (5) is rewritten with  $m = 4$  as

$$\frac{d^2 N_\gamma}{dE_\gamma^* d\Omega^*} = \frac{\bar{N}_\gamma \Theta_C}{4\pi T_C} \frac{(1-x^*)^4}{1+\zeta\tau_\theta^*} e^{-\tau_\theta^* x^*}, \quad (11)$$

which is useful, practically, for the comparison with experimental data in the CMS as presented in the next section.

Remembering the invariant phase space,  $E_\gamma^* dE_\gamma^* d\Omega^* = E_\gamma dE_\gamma d\Omega$ , the above equation gives the distribution function in LS as

$$\frac{d^2 N_\gamma}{dE_\gamma d\Omega} = \frac{\bar{N}_\gamma \Theta_C \beta_C^2}{2\pi M_P} \frac{(1-x\Gamma_\theta)^4}{\Gamma_\theta + \zeta\tau_\theta} e^{-\tau_\theta x}, \quad (12)$$

with  $x = E_\gamma/E_0$ , and

$$\tau_\theta = 2(\gamma_C^2 - 1)(M_P/p_0) \sin \theta, \quad (13)$$

$$\Gamma_\theta = 2(\gamma_C^2 - 1)(1 - \beta_C \cos \theta), \quad (14)$$

note  $\Gamma_\theta \approx 1 + \gamma_C^2 \theta^2$  for  $E_0 \gg M_P$  in the forward region, leading to  $x \approx x^*$ .

### 2.4. Average transverse momentum and inelasticity

In this subsection, we give the average transverse momentum of  $\gamma$ -rays using Eq. (11) (or Eq. [5]), which is a critical parameter in the multiple meson production, with a quite stable value, say 150 MeV/c, almost independent of the interaction energy. It is immediately given by

$$\frac{\bar{p}_t}{p_0} = \Theta_C \int_0^1 \tau_\theta^* \frac{F_1(\tau_\theta^*)}{1 + \zeta\tau_\theta^*} d(\cos \theta^*). \quad (15)$$

The total energy flow transferred to  $\gamma$ -rays in the CMS,  $\Sigma E_\gamma^*$ , is similarly obtained from Eq. (11),

$$\frac{\Sigma E_\gamma^*}{\bar{N}_\gamma T_C} = \frac{\bar{E}_\gamma^*}{T_C} = \Theta_C \int_0^1 \frac{F_1(\tau_\theta^*)}{1 + \zeta\tau_\theta^*} d(\cos \theta^*), \quad (16)$$

where  $\bar{E}_\gamma^*$  is the average energy of  $\gamma$ -rays in the CMS. In Fig. 3, we present  $\bar{p}_t/p_0$  and  $\bar{E}_\gamma^*/T_C$  simultaneously against  $\tau_C$  for several choices of  $\zeta$ , corresponding to Fig. 2.

Defining the average inelasticity transferred to  $\gamma$ -rays in the CMS,

$$\bar{k}_\gamma^* = \frac{\Sigma E_\gamma^*}{\sqrt{s} - 2M_P}, \quad (17)$$

we have

$$\bar{k}_\gamma^* = \frac{\bar{N}_\gamma \Theta_C}{2} \int_0^1 \frac{F_1(\tau_\theta^*)}{1 + \zeta \tau_\theta^*} d(\cos \theta^*), \quad (18)$$

where we use the approximation  $\sqrt{s} \gg 2M_p$  for the practical purpose. Assuming  $\bar{k}_{\text{tot}}^* = 1/2$  (total inelasticity) and  $p_{\pi^0} = 1/3$  (isospin symmetry), we expect  $\bar{k}_\gamma^* = 1/6$ , which is discussed again in Section 4.

### 2.5. Pseudo-rapidity distribution

Practically in the accelerator data, we often use a variable of pseudo-rapidity  $\eta^*$  instead of  $\theta^*$ , defined by  $\eta^* = -\ln \tan \theta^*/2$ . The pseudo-rapidity distribution is immediately given by, after integrating with respect to  $x^*$  in Eq. (11),

$$\frac{dN_\gamma}{d\eta^*} = \frac{\bar{N}_\gamma \Theta_C}{2 \cosh^2 \eta^*} \frac{F_0(\tau_\eta^*)}{1 + \zeta \tau_\eta^*}; \quad \tau_\eta^* = \frac{\tau_C}{\cosh \eta^*}. \quad (19)$$

It is also important to see the energy flow,  $d(\Sigma E_\gamma^*)$ , transferred to  $\gamma$ -rays within  $(\eta^*, \eta^* + d\eta^*)$ , which is given by

$$\frac{d(\Sigma E_\gamma^*)}{T_C d\eta^*} = \frac{\bar{N}_\gamma \Theta_C}{2 \cosh^2 \eta^*} \frac{F_1(\tau_\eta^*)}{1 + \zeta \tau_\eta^*}, \quad (20)$$

see Table 2 for  $F_0(\tau)$  and  $F_1(\tau)$ . The energy flow,  $d(\Sigma E_\gamma)$ , in LS within  $(\eta^*, \eta^* + d\eta^*)$  is easily given by

$$\frac{d(\Sigma E_\gamma)}{d\eta^*} = \frac{\cosh(\eta^* + \eta_C)}{\cosh \eta^*} \frac{d(\Sigma E_\gamma^*)}{d\eta^*}, \quad (21)$$

with  $\eta_C = \frac{1}{2} \ln(1 + \beta_C)/(1 - \beta_C)$ , i.e., rapidity of the CMS against the LS. One finds a reasonable relation between the total energy flow in LS and that in the CMS,  $\Sigma E_\gamma = \gamma_C \Sigma E_\gamma^*$ , after integrating both sides of Eq. (21) over  $\eta^*$  (see Eq. [16] for the explicit form of  $\Sigma E_\gamma^*$ ) because of the forward-backward symmetry in the CMS, leading to  $\bar{k}_\gamma \approx \bar{k}_\gamma^*$ .

In Fig. 4, we demonstrate three kinds of density distribution against  $\eta^*$  simultaneously,  $\rho_N^*$  (multiplicity),  $\rho_E^*$  (energy flow in CMS), and  $\rho_E$  (energy flow in LS), for  $E_0 = 10^{11}, 10^{14}, 10^{17}$  eV, where the vertical axis is normalized to unity after integrating over  $\eta^*$ ,

$$\rho_N^* = \frac{dN_\gamma}{\bar{N}_\gamma d\eta^*}, \quad \rho_E^* = \frac{d(\Sigma E_\gamma^*)}{\Sigma E_\gamma^* d\eta^*}, \quad \rho_E = \frac{d(\Sigma E_\gamma)}{\Sigma E_\gamma d\eta^*}. \quad (22)$$

Figure 3: Numerical values of  $\bar{p}_t/p_0$  and  $\bar{E}_\gamma^*/T_C$  against  $\tau_C$  for several choices of  $\zeta$ , where the former corresponds to the left axis, and the latter to the right axis respectively.



Figure 4: Three kinds of density distribution (see Eq. [22]) against the pseudo-rapidity  $\eta^*$  in the differential form, a) multiplicity, b) energy flow in CMS, and c) energy flow in LS, for three energies,  $E_0 = 10^{11}$ ,  $10^{14}$ , and  $10^{17}$  eV.

Figure 5: Three kinds of density distribution against the pseudo-rapidity  $\eta^*$  in the integral form, corresponding to those in the differential form presented in Fig. 4.

On the other hand, we present the integral forms for three kinds of density,  $P_N^*(\geq\eta^*)$ ,  $P_E^*(\geq\eta^*)$ , and  $P_{LE}(\geq\eta^*)$  in Fig. 5, corresponding to Fig. 4. From these figures, one finds that the energy flow in LS comes from mostly those produced in the very forward region in CMS, particularly for higher energy. This means that essential is the production energy spectrum of  $\gamma$ -rays in the very forward region in CMS, contrarily not important in the central region, and of much less importance in the backward.

While the present paper is focussed upon the  $\gamma$ -ray component produced by  $\pi^0$ -decay, the pseudo-rapidity distributions of *charged hadrons*,  $dN_{\text{ch}}/d\eta^*$ , have been extensively studied with accelerator experiments, closely related to  $dN_\gamma/d\eta^*$  given by Eq. (19). So we present the kinematical relation between them rather in detail in Appendix A, which is given by, assuming  $\bar{N}_\gamma \approx \bar{N}_{\text{ch}}$ ,

$$\frac{dN_{\text{ch}}}{d\eta^*} \approx \left[ 1 + \frac{1}{2} \left( \frac{m_{\pi^0}}{p_0} \right)^2 \frac{\Delta(\eta^*)}{F_0(\tau_{\eta^*})} \tanh^2 \eta^* \right] \frac{dN_\gamma}{d\eta^*}, \quad (23)$$

where  $m_{\pi^0}$  is the mass of  $\pi^0$ , and see Eq. (A12) in the appendix for  $\Delta(\eta^*)$ .

### 3. Comparison with experimental data

In this section, we determine two parameters appearing in Eq. (5),  $[\bar{N}_\gamma, p_0]$ , while the other two,  $[m, \zeta]$ , are fixed to  $[4, 0.02]$  as mentioned in Section 2.2. Now the average transverse momentum  $\bar{p}_t$  is quite stable, and well established in both accelerator and CR experiments with  $150 \sim 200$  MeV/c. So we use the parameter  $\bar{p}_t$  in place of  $p_0$ , which is given by Eq. (15),

$$\frac{\bar{p}_t}{p_0} = \int_0^1 \tau_\theta^* \frac{F_1(\tau_\theta^*)}{1 + \zeta \tau_\theta^*} d(\cos \theta^*) \bigg/ \int_0^1 \frac{F_0(\tau_\theta^*)}{1 + \zeta \tau_\theta^*} d(\cos \theta^*), \quad (24)$$

while we have to solve numerically the above transcendental equation, with respect to  $p_0$ , note that it also appears in  $\tau_\theta^* = \tau_c \sin \theta^* = T_c \sin \theta^* / p_0$  in the right-hand side of Eq. (24). In practice,  $p_0$  is easily obtained by the iteration

Figure 6: Energy spectrum of  $\gamma$ -rays at  $E_0 = 0.97$  GeV [14]. Empirical curves are given by Eq. (12) after integrating over  $\cos \theta$ .

Figure 7: Energy spectrum of  $\gamma$ -rays at  $E_0 = 23.1$  GeV [15] for different emission angles. Empirical curves are given by Eq. (12).

method with the initial value of 200 MeV/c for the set of  $[E_0, \bar{p}_t]$  (or  $[T_c, \bar{p}_t]$ ), since  $p_0$  is also quite stable with 150-250 MeV/c for  $\bar{p}_t = 100$ -230 MeV/c (see Figs. 3 and 17).

Explicit values of  $[\bar{N}_\gamma, \bar{p}_t]$  are presented in each figure appearing in the following subsections (see also Figs. 16 and 17, and Table 3), which are obtained by fitting the experimental data with the present empirical curve.

### 3.1. The low energy region ( $E_0 = 1 - 300$ GeV)

From Eq. (12), we can obtain easily the energy distribution in LS integrating over  $\cos \theta$ . In Fig. 6, we compare the empirical one thus obtained with the data at  $E_0 = 0.97$  GeV given by Bugg et al. [14]<sup>1</sup>, and find that they are well reproduced with the numerical values of  $\bar{N}_\gamma$  and  $\bar{p}_t$  presented in the figure.

Fidecaro et al. [15] gave the production cross-section of  $\gamma$ -rays for different emission angles at  $E_0 = 23.1$  GeV in the LS, which is presented in Fig. 7 together with curves expected from Eq. (12). One finds the agreement is excellent for all emission angles.

In Fig. 8, we show the energy distribution with use of the Feynman variable,  $x_F^* = x^* \cos \theta^*$ , at two energies,  $E_0 = 11.5, 203.7$  GeV [16, 17]. Empirical curves are obtained by replacing  $x^*$  with  $x_F^* \sec \theta^*$  in Eq. (11), where we must take care of the integral range for  $\cos \theta^*$  with  $x_F^* \leq \cos \theta^* \leq 1$ . One finds the empirical ones reproduce well both data. In Fig. 9, we present the pseudorapidity distributions at  $E_0 = 11.5, 203.7, \text{ and } 299.1$  GeV [16, 17, 18], together with the empirical ones obtained by Eq. (19). Our numerical curves are again in nice coincidence with the data.

### 3.2. The high energy region ( $E_0 = 0.5 - 200$ TeV)

In this subsection, we compare the experimental data in TeV region with our cross-section given by Eq. (5), which are obtained by ISR, FNAL, and

---

<sup>1</sup>Original data were given in the form of the production cross-section for  $\pi^0$ ,  $\sigma_{pp \rightarrow \pi^0}(E_0, E_{\pi^0})$ . As they gave explicitly the number of events per 25 MeV energy bin, we converted them into  $\sigma_{pp \rightarrow \gamma}(E_0, E_\gamma)$  by randomly sampling for the  $\pi^0 \rightarrow 2\gamma$  decay in each energy bin.

Figure 8: Production cross-section of  $\gamma$ -rays with use of the Feynman scaling variable  $x_{\mathbb{F}}^*$  at two energies,  $E_0 = 11.5, 203.7$  GeV [16, 17].

Figure 9: Pseudo-rapidity distributions at three energies,  $E_0 = 11.5, 203.7, 299.1$  GeV [16, 17, 18]. Empirical curves are obtained by Eq. (19).

Figure 10: Energy spectrum of  $\gamma$ -rays for several sets of the emission angle in the CMS at ISR energies [19]. Empirical curves are given by Eq. (11).

the Chacaltaya EC with CR-beams. In Fig. 10, we present the ISR data [19] with  $\sqrt{s} = 30.2, 44.7, \text{ and } 52.7$  GeV, each corresponding to  $E_0 = 0.483, 1.06, 1.48$  TeV in the LS respectively, where empirical curves are obtained by Eq. (11). One might worry about some discrepancies appearing in the low energy region,  $E_{\gamma}^* \lesssim 1$  GeV, but it is not so critical in the practice as mentioned in Section 2.5, namely important is only the high energy part in the forward region in CMS, see Fig. 5.

As presented in Paper I, the Chacaltaya EC data [20] provide the fractional energy spectrum of  $\gamma$ -rays,  $f_{\gamma} = E_{\gamma}/\Sigma E_{\gamma}$ , in  $E_0 = 30 - 200$  TeV region. The relation between  $\Sigma E_{\gamma}$  and  $E_0$  is given by assuming the  $\gamma$ -ray inelasticity,  $\bar{k}_{\gamma}$ , while we have to take care of the bias-effect in EC experiments ( $\bar{k}_{\gamma, \text{bias}} = 0.28$ ), see Paper I for the detail. In Fig. 11, we show the  $f_{\gamma}$ -spectrum for both data and curves expected from Eq. (12) after integrating over the emission angle.

Figure 11: Fractional energy spectrum of  $\gamma$ -rays obtained by Chacaltaya EC experiments [20] for three energy flow ranges,  $\Sigma E_{\gamma} = 7-10, 10-20, \text{ and } 20-50$  TeV, each corresponding to the average energy for projectile proton,  $\langle E_0 \rangle = 29.2, 45.1, \text{ and } 101.2$  TeV respectively.

Figure 12: Pseudo-rapidity distributions obtained by UA7 [22], and the Chacaltaya EC experiments [20]. Empirical curves are given by Eq. (19).

Figure 13: Pseudo-rapidity distributions of charged hadrons obtained by UA5 [21]. Empirical curves are given by Eq. (23).

The agreement is quite well within the statistical error.

We present the pseudo-rapidity distribution in Fig. 12 obtained by UA7 [22], and EC data [20], where we present the curve expected from Eq. (19) with  $\sqrt{s} = 600$  GeV. Again we find that the present curve reproduces nicely the data.

In Fig. 13, we show the pseudo-rapidity distribution of charged hadrons obtained by UA5 [21], for three energies,  $\sqrt{s} = 52.7, 200,$  and  $546$  GeV. The numerical curves are given by Eq. (23) with the assumption of  $\bar{N}_{\text{ch}} = \bar{N}_{\gamma}$ , taking the  $\pi^0 \rightarrow 2\gamma$  decay into account. We find that they are in good agreement with the UA5 data.

### 3.3. The LHC energy region ( $E_0 = 0.4 - 30$ PeV)

Now we compare our production cross-section with the LHC data most recently reported, while the final goal with  $\sqrt{s} = 14$  TeV will be available around 2014. LHCf group [4] present recently the energy spectra of  $\gamma$ -rays in the very forward region,  $\eta^* \gtrsim 8.8$ , at  $\sqrt{s} = 7$  TeV, corresponding to  $E_0 = 26$  PeV in the LS. Let us apply our formula given by Eq. (11) for LHCf data, and estimate  $[\bar{N}_{\gamma}, \bar{p}_t]$ .

In Fig. 14, we give the energy spectra at  $\sqrt{s} = 7$  TeV, for two sets of  $[\Delta\eta^*, \Delta\phi^*]$ , (a)  $[\eta^* > 10.94, 360^\circ]$  and (b)  $[8.81 < \eta^* < 8.99, 20^\circ]$ , where two curves from our empirical cross-section are presented together. We find that they reproduce well the experimental data in spectral shape, but the absolute value of  $\bar{N}_{\gamma}$  (average photon yield) is of approximately 20% difference between them, 53.4 for (a) and 68.0 for (b), while the latter is consistent with 71.5 expected from TOTEM with the pseudo-rapidity distribution of charged hadrons (see Fig. 15), assuming  $\bar{N}_{\gamma} \approx \bar{N}_{\text{ch}}$ .

In addition to the energy spectra of  $\gamma$ -rays in the forward region obtained by the LHCf group, UA5 [21], ALICE [23] and TOTEM [24] present the pseudo-rapidity distribution of charged hadrons in the central region as shown in Fig. 15, covering the energies  $\sqrt{s} = 900$  GeV, 2.36 TeV, and 7 TeV, where numerical curves are obtained by Eq. (23) with the assumption of  $\bar{N}_{\gamma} \approx \bar{N}_{\text{ch}}$ . One

Figure 14: Energy spectrum of  $\gamma$ -rays obtained by LHCf at  $\sqrt{s} = 7$  TeV for two sets of  $[\Delta\eta^*, \Delta\phi^*]$ , (a)  $[\eta^* > 10.94, 360^\circ]$  and (b)  $[8.81 < \eta^* < 8.99, 20^\circ]$ , where separately presented are two detectors, Arm1 (open circle) and Arm2 (filled circle), each with the scintillation fiber and the silicon strip respectively.

Figure 15: Pseudo-rapidity distribution of charged hadrons obtained by UA5 [21], ALICE [23], and TOTEM [24] at  $\sqrt{s} = 900$  GeV, 2.36 TeV, and 7 TeV, where curves are given by Eq. (23), assuming  $\bar{N}_\gamma \approx \bar{N}_{\text{ch}}$ .

finds that they are well in consistent with the experimental data, particularly interesting is that the concave shape around  $\eta^* \approx 0$  is nicely reproduced.

Table 3: Summary of  $[\bar{N}_\gamma, \bar{p}_t]$ , where LHCf-1 corresponds to the data with  $[\eta^* > 10.94, \Delta\phi^* = 360^\circ]$ , and LHCf-2 to those with  $[8.81 < \eta^* < 8.99, \Delta\phi^* = 20^\circ]$ , and “(n)” ( $n = 0, 1, 2, \dots$ ) appearing in the column of  $E_0$  denotes “ $10^n$ ”. Fig.13 and Fig.15 with asterisk mark correspond to the data from the pseudo-rapidity distribution of charged hadrons, assuming  $\bar{N}_\gamma \approx \bar{N}_{\text{ch}}$  and  $\bar{p}_t(\gamma) \approx \bar{p}_t(\pi)/2$ .

Figure :	Data reference	$\sqrt{s}$ (GeV)	$E_0$ (GeV)	$N_\gamma$	$\bar{p}_t$ (MeV/c)
Fig. 6 :	Bugg et al. [14]	2.31	0.97(0)	$0.32 \pm 0.11$	$102 \pm 32$
Fig. 7 :	Fidecaro et al. [15]	6.85	2.31(1)	$3.50 \pm 0.28$	$137 \pm 9$
Fig. 8 :	Jager et al. [16]	5.02	1.15(1)	$1.68 \pm 0.27$	$120 \pm 16$
	Jager et al. [17]	19.7	2.04(2)	$8.25 \pm 0.93$	$167 \pm 16$
Fig. 9 :	[16]	5.02	1.15(1)	$2.33 \pm 0.20$	$125 \pm 9$
	[17]	19.7	2.04(2)	$7.45 \pm 0.74$	$167 \pm 18$
	Shenger et al. [18]	23.7	2.99(2)	$7.75 \pm 0.70$	$155 \pm 16$
Fig. 10 :	ISR [19]	30.2	4.83(2)	$7.80 \pm 0.81$	$141 \pm 15$
		44.7	1.06(3)	$9.02 \pm 1.09$	$136 \pm 17$
		52.7	1.48(3)	$9.65 \pm 1.03$	$138 \pm 15$
Fig. 11 :	Chacaltaya [20]	234.	2.92(4)	$23.0 \pm 4.17$	$189 \pm 34$
		291.	4.51(4)	$24.8 \pm 4.92$	$190 \pm 38$
		436.	1.01(5)	$35.0 \pm 4.49$	$229 \pm 29$
Fig. 12 :	[20], UA7 [22]	615.	2.04(5)	$30.4 \pm 3.52$	$211 \pm 17$
Fig. 13*:	UA5 [21]	52.7	1.48(3)	$12.2 \pm 2.55$	$146 \pm 31$
		200.	2.13(4)	$19.2 \pm 3.05$	$170 \pm 36$
		546.	1.59(5)	$25.3 \pm 3.28$	$183 \pm 30$
Fig. 14 :	LHCf-1 [4]	7000	2.61(7)	$53.4 \pm 5.58$	$234 \pm 25$
	LHCf-2 [4]	7000	2.61(7)	$68.0 \pm 7.02$	$234 \pm 25$
Fig. 15*:	[24], [23], [21]	900.	4.31(5)	$31.9 \pm 7.01$	$183 \pm 30$
	[24], ALICE [23]	2360	2.96(6)	$46.9 \pm 9.87$	$203 \pm 20$
	TOTEM [24]	7000	2.61(7)	$71.5 \pm 15.0$	$222 \pm 20$

Figure 16: The total production cross-section of  $\gamma$ -rays,  $\bar{N}_\gamma\sigma_{\text{pp}}$ , against the proton kinetic energy  $E_0$ , where those compiled by Stecker [3] (filled squares) are plotted together. The present curve (solid curve) is obtained by Eq. (1) for  $\sigma_{\text{pp}}$  and Eq. (25) for  $\bar{N}_\gamma$  respectively, where the previous one (dashed curve) is also presented.

Figure 17: Average transverse momentum of  $\gamma$ -rays against  $E_0$ , where we present also those expected from charged pions (open circles) [37] with the assumption of  $\bar{p}_t(\gamma) \approx \bar{p}_t(\pi)/2$ .

### 3.4. The multiplicity and the average transverse momentum

In Figs. 6-15, we present explicitly the numerical sets of  $[\bar{N}_\gamma, \bar{p}_t]$  in the extremely wide energy ranges,  $E_0 = 1 \text{ GeV} \sim 26 \text{ PeV}$ , which are summarized all together in Table 3.

For the  $\gamma$ -ray astronomy, practically the most essential is the *total* production cross-section of  $\gamma$ -rays,  $\bar{N}_\gamma \times \sigma_{\text{pp}}$ , no matter how the emission-angle  $\theta^*$  (or the transverse momentum  $p_t$ ) appears in the functional form of the cross-section. After Stecker [3] summarized it in 1973, we revised it in Paper I with the data covering TeV region but without LHC data.

Let us present  $\bar{N}_\gamma\sigma_{\text{pp}}$  against  $E_0$  in Fig. 16 with LHC data, using Eq. (1) for  $\sigma_{\text{pp}}(E_0)$ , where we give a solid curve obtained by the following empirical form for  $\bar{N}_\gamma$ ,

$$\bar{N}_\gamma(E_0) = \bar{N}_0 \hat{E}_0^{0.115} \left[ 1 - \exp\left(-0.47\sqrt{\hat{E}_0}\right) \right], \quad (25a)$$

$$\bar{N}_0(E_0) = 8.80 \times \left[ 1 - \exp\left(-0.15\sqrt[4]{\hat{E}_0}\right) \right], \quad (25b)$$

with  $\hat{E}_0 = E_0 - 2m_\pi$  in GeV, and presented together is a dashed curve from the previous parametrization [1] for  $\bar{N}_\gamma(E_0)$ . We plot also  $\bar{N}_\gamma\sigma_{\text{pp}}$  (open circles) expected from the pseudo-rapidity distribution of charged hadrons, assuming  $\bar{N}_\gamma \approx \bar{N}_{\text{ch}}$  (see Figs. 13 and 15).

One finds that the previous one gives significantly over-estimation in PeV region, and the present one reproduces nicely the experimental points in the very wide energy range,  $E_0 = 1 \text{ GeV} \sim 26 \text{ PeV}$ .

Figure 18: The average inelasticity,  $\bar{k}_\gamma^*$  transferred to  $\gamma$ -rays against  $E_0$ , where also plotted are those expected from the charged hadrons (filled squares) with the assumption of  $\bar{k}_\gamma^* \approx \bar{k}_{\text{ch}}^*/2$ .

In Fig. 17, we give the average transverse momentum,  $\bar{p}_t$ , against  $E_0$ , together with the empirical curve given by

$$\bar{p}_t(E_0) = \bar{p}_0 \hat{E}_0^{0.0286} \left[ 1 - \exp\left(-1.156 \sqrt[4]{\hat{E}_0}\right) \right], \quad (26)$$

with

$$\bar{p}_0 = m_\pi c = 140 \text{ MeV}/c,$$

while it is of little interest for the  $\gamma$ -ray astronomy, but important for the study of shower phenomena in the atmosphere. In Fig. 17 we plot also the half of the transverse momentum of the charged pions [37], assuming  $\bar{p}_t(\gamma) \approx \bar{p}_t(\pi)/2$ . One finds that  $\bar{p}_t$  increases slowly with  $E_0$ , as given by Eq. (26).

#### 4. Discussions

In the present paper, interpolating experimental data nowadays covering the very wide energy range from GeV to 30 PeV, we have focussed our work on the construction of the semi-empirical formula for the inclusive production cross-section of  $\gamma$ -rays,  $\sigma_{\text{pp} \rightarrow \gamma}(E_0, E_\gamma)$ , without asking for the cumbersome QCD-based models, and find that it reproduces excellently the machine data over the very wide energy ranges.

The present simple parameterization in the formula should be compared to the simulation codes currently available in the CR community, which are usually very complicated, patching different models separately in low and high energy regions, and *heavy* in the sense that they are constructed so that all the components ( $\pi^\pm, \pi^0, K^\pm, \dots$ ) in both soft (small  $q^2$ ) and hard (large  $q^2$ ) processes simultaneously match with the accelerator data. So it is not an easy task for physicists other than a developer of simulation code to improve it freely, by contrast with the empirical formula, quite easy to touch the parameters appearing there. Of course one should keep in mind that our approach (interpolation method) is not valid for the study of extremely high energy shower phenomena in the atmosphere, say  $\gtrsim 10^{18}$  eV, where even the LHC can not cover, resulting in the need of some theoretical models in order to extrapolate the LHC data much higher, while the present parameterization is valid enough for the future  $\gamma$ -ray astronomy, even up to PeV- $\gamma$  observation.

We have concentrated our interest upon two parameters,  $\bar{N}_\gamma$  and  $\bar{p}_t$ , particularly on the former. As mentioned often, the multiplicity  $\bar{N}_\gamma$  plays an essential

role for the study of  $\gamma$ -ray astronomy, appearing always in the form of the total production cross-section,  $\bar{N}_\gamma(E_0) \times \sigma_{\text{pp}}(E_0)$  as presented in Fig. 16.

Alternatively,  $\bar{N}_\gamma$  is important also for the study of the shower phenomena in the atmosphere, appearing in the (total) inelasticity  $\bar{k}_{\text{tot}}$  ( $\approx \bar{k}_{\text{tot}}^*$ ). So let us present  $\bar{k}_\gamma^*$  (see Eq. [18]) transferred to  $\gamma$ -rays against  $E_0$  in Fig. 18, where also plotted are those (filled squares) expected from charged hadrons (see Figs. 13 and 15), assuming  $\bar{k}_\gamma^* \approx \bar{k}_{\text{ch}}^*/2$ . An error-bar attached to each square comes from statistical ones to  $\bar{N}_\gamma$  as presented in Fig. 16. One finds approximately  $\bar{k}_\gamma^* \approx 1/6$  as a whole, almost independent of  $E_0$ , while it is as small as 0.1-0.17 in the low energy region  $E_0 \lesssim 1$  TeV, and as large as 0.15-0.2 in the high energy region  $\gtrsim 10$  TeV, indicating a small increase as the energy gets higher. But we reserve the conclusion for future studies, either constant or the increase.

It has been well-known that the attenuation length  $A$  for the intensity of CR hadronic components in the atmosphere is given by  $\lambda/A = 1 - \langle (1 - k_{\text{tot}})^\beta \rangle$  [25], where  $\lambda$  is the collision length, and  $\beta$  the index of the integral primary CR spectrum with  $\sim 1.8$ . Experimentally we have  $A/\lambda \approx 1.5$ , with for instance  $\lambda \approx 70$  g/cm<sup>2</sup> and  $A \approx 100$  g/cm<sup>2</sup> [27], leading to  $\bar{k}_{\text{tot}} \approx 1/2$  in the energy region  $E_0 \lesssim 100$  TeV, assuming the uniform distribution in  $k_{\text{tot}}$ , while not yet clear in the air shower region  $E_0 \gtrsim 10$  PeV. Anyway the present result is not inconsistent with the common understanding in the inelasticity expected from the attenuation of CRs in the atmosphere.

Finally we address further two open problems in the present paper; (1) the nucleus effect of proton-nucleus (p-A) and/or nucleus-nucleus (A-A) collisions for the production cross-section of  $\gamma$ -rays in p-p collisions, and (2) the applicability of the present empirical cross-section for the galactic phenomena other than emissions of the hadron-induced  $\gamma$ -rays, particularly for those of the electron-positrons coming from  $\pi-\mu-e$  decays.

First, for the problem (1), one should remember that the effective  $\gamma$ -rays produced by the nuclear interaction in the galactic environments (either in ISM or in SNR) are only those produced in the forward region in the CMS, while not important are those in the central and backward regions. The effect of the plural interactions inside the nucleus appears only in the latter regions. In fact, it has been experimentally well-known that the difference between those produced by p-p and those by p-A (A-A) collisions appears only in the latter regions, while they are well in coincidence with each other in the forward region. This is the reason why we present Fig. 5, stressing in the present paper how essential are the  $\gamma$ -rays produced in the forward region, in contrast not important in the central region, and of much less importance in the backward.

Practically, of course, we need the production cross-section of  $\gamma$ -rays for p-A (A-A) collisions, as there exist additionally helium and heavier components in CRs (projectiles) as well as the helium gas in the ISM (targets), while unfortunately we have not yet a reliable model nowadays for the p-A (A-A) collisions. We have used the modified wounded-nucleon model of Gaisser and Schafer [34] in our past calculations [26, 27], where we mention that the uncertainty in the nu-



cleus effect is of the second order for the practice. In order to see the uncertainty, we have introduced so called the “enhancement factor” defined by  $\epsilon_q = q_{\text{all}}/q_{\text{pp}}$ , taking the energy dependence into account, where  $q_{\text{all}}$  is the emissivity of  $\gamma$ -rays in the galaxy produced by all kinds of nuclear interactions with p-p, p-A and A-A, and  $q_{\text{pp}}$  by those with p-p only. For instance,  $\epsilon_q = 1.54$  (Gaisser-Shafer [34]), 1.50 (Cavallo-Gould [35]), 1.60 (Stephens-Badhwar [36]), and 1.53 (Shibata et al. [26]), indicating that the difference in the choice of nucleus interaction model is not so significant as compared to that in the choice of the propagation model. These results tell us also that the procedure in the calculation of the CR propagation becomes quite simple by the use of the enhancement factor  $\epsilon_q$ .

Second, for the problem (2), indeed we do not touch the intermediate meson,  $\pi^0$ , except the pseudo-rapidity distribution of charged hadrons (Figs. 13 and 15), but the decay products  $\gamma$ 's only, having no interest in the intermediate mesons, either via  $\pi^0$  or via heavier  $\eta, \eta'$ , etc.. However, as long as focussing on the decay products such as electrons and/or neutrinos from muons, the present empirical form for  $\gamma$ 's,  $\sigma_{\text{pp}\rightarrow\gamma}(E_0, E_\gamma)$ , is valid also for muons produced via pions,  $\sigma_{\text{pp}\rightarrow\mu}(E_0, E_\mu)$ , while we have to take care of the mass difference between photon and the muon. This is because both decays,  $\pi^0 \rightarrow \gamma + \gamma$  and  $\pi^\pm \rightarrow \mu^\pm + \nu(\bar{\nu})$ , are isotropic two-body decays in the pion rest system, leading to the same kinematics in  $\gamma$  and  $\mu^\pm$  but different mass. Namely, we do not need the information of the intermediate pions also in the case of the muon production cross-section. This fact tells us that we have model-independently a kinematical relation between the emissivity of  $\gamma$ -rays and that of (secondary) electron-positrons in the galaxy, detail of which will be reported elsewhere in connection with the galactic electron-positron spectrum.

In the near future, we will apply the present cross-section,  $\sigma_{\text{pp}\rightarrow\gamma}(E_0, E_\gamma)$ , for the observational data in TeV region currently available on both diffused  $\gamma$ -rays and those from the source, while one of the authors (T. S.) have studied the former components in *Fermi* energy region, 100 MeV  $\sim$  100 GeV [26], [27], using the old parameterization in  $\sigma_{\text{pp}\rightarrow\gamma}(E_0, E_\gamma)$ .

## 5. Acknowledgements

We thank T. Sako (Nogoya University) for giving us valuable information and comments on LHCf experiments. We are also grateful to CTA-Japan member for valuable discussions in the internal meetings.

### Appendix A: Kinematical relation between $\gamma$ and $\pi^0$ angular-distributions

The kinematical relation between  $\gamma$  and  $\pi^0$  energy-distributions was studied by Sternheimer [32], where he assumed that the opening angle,  $\alpha^*$ , of two  $\gamma$ 's from the decay of high energy  $\pi^0$  is so small that the emission angle of  $\gamma$  is approximately equal to that of  $\pi^0$ ,  $\theta_\gamma^* \approx \theta_{\pi^0}^*$ . But this approximation seems to be too rough to transform practically from the pseudo-rapidity distribution of  $\gamma$ 's to that of  $\pi^0$ 's, namely  $dN_\gamma/d\eta^* = 2dN_{\pi^0}/d\eta^*$  in his approximation. In this appendix we present a more realistic relation between them.

Let us consider a  $\pi^0$  produced by p-p collision with  $(E_{\pi^0}^*, \theta_{\pi^0}^*, \phi_{\pi^0}^*)$ , each denoting the energy, emission angle, and the azimuthal angle in the CMS respectively, and disintegrate into two  $\gamma$ 's with  $(E_1^*, \theta_1^*, \phi_1^*)$  and  $(E_2^*, \theta_2^*, \phi_2^*)$ , where individual angles are those against the collision axis. We define further two sets of angles,  $(\Theta_1^*, \Phi_1^*)$  and  $(\Theta_2^*, \Phi_2^*)$ , which are the emission angles and the zenith angles of two  $\gamma$ 's against the *moving direction* of  $\pi^0$ . In this appendix we put  $c = 1$  for the sake of simplicity.

We have following relations in these variables

$$E_1^* + E_2^* = E_{\pi^0}^*, \quad (\text{A1a})$$

$$\Theta_1^* + \Theta_2^* = \alpha^*, \quad (\text{A1b})$$

$$E_1^* \sin \Theta_1^* = E_2^* \sin \Theta_2^*, \quad (\text{A1c})$$

and

$$\cos \theta_1^* = \cos \Theta_1^* \cos \theta_{\pi^0}^* + \sin \Theta_1^* \sin \theta_{\pi^0}^* \cos \Phi_1^*. \quad (\text{A2})$$

Integrating over  $\Phi_1^*$  for both sides of Eq. (A2), we have

$$\langle \cos \theta_1^* \rangle = \cos \Theta_1^* \cos \theta_{\pi^0}^*, \quad (\text{A3})$$

and hereafter we omit angle brackets,  $\langle \dots \rangle$ , in the left-hand side for the simplicity, as we are not interested in the azimuthal component.

Remembering a well-known relation in  $\pi^0$ -decay [33]

$$\alpha^* \approx \frac{m_{\pi^0}}{\sqrt{E_1^* E_2^*}} = \frac{m_{\pi^0}}{\sqrt{E_1^* (E_{\pi^0}^* - E_1^*)}}, \quad (\text{A4})$$

for  $E_{\pi^0}^* \gg m_{\pi^0}$ , we obtain, from Eqs. (A1a)-(A1c),

$$\Theta_1^* \approx \frac{m_{\pi^0}}{E_{\pi^0}^*} \sqrt{\frac{E_{\pi^0}^*}{E_1^*} - 1},$$

namely

$$\cos \Theta_1^* \approx 1 - \omega(E_{\pi^0}^*, E_1^*),$$

with

$$\omega(E_{\pi^0}^*, E_1^*) = \frac{1}{2} \left( \frac{m_{\pi^0}}{E_{\pi^0}^*} \right)^2 \left( \frac{E_{\pi^0}^*}{E_1^*} - 1 \right).$$

Now we have from Eq. (A3), putting  $\theta_\gamma^* \equiv \theta_1^*$  and  $E_\gamma^* \equiv E_1^*$ ,

$$\cos \theta_{\pi^0}^* \approx \left\{ 1 + \omega(E_{\pi^0}^*, E_\gamma^*) \right\} \cos \theta_\gamma^*. \quad (\text{A5})$$

Here we have to take care of the above expansion with respect to  $\omega$ , which is based on the approximation with  $\theta_{\pi^0}^* \gg \alpha^*$ , while Sternheimer assumed  $\alpha^* \approx 0$

[32]. This means the energy range of  $\gamma$  is limited within  $(E_-^*, E_+^*)$  for the fixed energy of  $\pi^0$ ,  $E_{\pi^0}^*$ , which are obtained from Eq. (A4) with  $\theta_{\pi^0}^* \geq \alpha^*$ , and given by

$$E_{\pm}^* = [1 \pm B(E_{\pi^0}^*, \theta_{\pi^0}^*)]E_{\pi^0}^*/2, \quad (\text{A6})$$

with

$$B(E_{\pi^0}^*, \theta_{\pi^0}^*) = \sqrt{1 - (2m_{\pi^0}/E_{\pi^0}^* \theta_{\pi^0}^*)^2}. \quad (\text{A7})$$

Now, we define the energy-angular distribution function of  $\pi^0$  with  $t_{\pi^0}^* \equiv \cos \theta_{\pi^0}^*$

$$n_{\pi^0}(E_{\pi^0}^*, t_{\pi^0}^*) \equiv \frac{d^2 N_{\pi^0}}{dE_{\pi^0}^* dt_{\pi^0}^*},$$

and thus the energy-angular distribution function of  $\gamma$  is given by, putting  $t_{\gamma}^* \equiv \cos \theta_{\gamma}^*$ ,

$$n_{\gamma}(E_{\gamma}^*, t_{\gamma}^*) = 2 \int_{E_{\gamma}^*}^{T_C} \frac{dE_{\pi^0}^*}{p_{\pi^0}^*} \int_{-1}^1 dt_{\pi^0}^* \delta \left[ t_{\pi^0}^* - \left\{ 1 + \omega(E_{\pi^0}^*, E_{\gamma}^*) \right\} t_{\gamma}^* \right] n_{\pi^0}(E_{\pi^0}^*, t_{\pi^0}^*), \quad (\text{A8})$$

and  $T_C$  is the maximum energy of  $\pi^0$  given by Eq. (6) in the text.

For  $E_{\pi^0}^* \gg m_{\pi^0}$  (equivalently  $\omega \ll 1$ ), we have with use of Eq. (A5)

$$n_{\pi^0}(E_{\pi^0}^*, t_{\pi^0}^*) \approx n_{\pi^0}(E_{\pi^0}^*, t_{\gamma}^*) + \omega(E_{\pi^0}^*, E_{\gamma}^*) t_{\gamma}^* \frac{\partial}{\partial t_{\gamma}^*} n_{\pi^0}(E_{\pi^0}^*, t_{\gamma}^*),$$

and integrating over  $E_{\gamma}^*$  for both sides of Eq. (A8) in order to obtain the angular distribution, we obtain

$$n_{\gamma}(t_{\gamma}^*) \approx 2n_{\pi^0}(t_{\gamma}^*) + 2t_{\gamma}^* \int_0^{T_C} dE_{\gamma}^* \int_{E_{\gamma}^*}^{T_C} \frac{dE_{\pi^0}^*}{p_{\pi^0}^*} \omega(E_{\pi^0}^*, E_{\gamma}^*) \frac{\partial}{\partial t_{\gamma}^*} n_{\pi^0}(E_{\pi^0}^*, t_{\gamma}^*), \quad (\text{A9})$$

where one has to take care of the kinematical constraints in  $(E_{\pi^0}^*, E_{\gamma}^*)$  given by Eqs. (A6) and (A7) for the practical integrations.

Now we use the approximation given by Sternheimer for  $n_{\pi^0}$  appearing in the integrand in Eq. (A9),

$$n_{\pi^0}(E_{\pi^0}^*, t_{\gamma}^*) \approx -\frac{1}{2} p_{\pi^0}^* \frac{\partial}{\partial E_{\pi^0}^*} n_{\gamma}(E_{\pi^0}^*, t_{\gamma}^*),$$

note that the second iteration for  $n_{\pi^0}$  is negligible as shown in Fig. 19, and next exchange the order of integrations for  $E_{\gamma}^*$  and  $E_{\pi^0}^*$ , taking care of the kinematical constraints mentioned before

$$\int_0^{T_C} dE_{\gamma}^* \int_{E_{\gamma}^*}^{T_C} dE_{\pi^0}^* \implies \int_{E_{\eta}^*}^{T_C} dE_{\pi^0}^* \int_{E_-^*}^{E_+^*} dE_{\gamma}^*$$

Figure 19: Correction rate for the Sternheimer approximation with  $\alpha^* \approx 0$ , corresponding to the second term in the square bracket in Eq. (A11) for  $\sqrt{s} = 0.1, 0.2, 0.5, 1.0$  TeV, where we assume  $p_0 = 200$  MeV/c for two choices of  $\zeta$ , 0.02 and 0.04.

with

$$E_{\eta^*} = 2m_{\pi^0}/\theta_{\gamma}^* = m_{\pi^0}/\tan^{-1}(e^{-\eta^*}).$$

The second term in the right-hand side of Eq. (A9) is thus given by

$$-\frac{m_{\pi^0}^2}{2T_{\text{C}}} \int_{x_{\eta^*}}^1 \frac{dx}{x} \left( \ln \frac{1+B_{x,\eta^*}}{1-B_{x,\eta^*}} - B_{x,\eta^*} \right) \frac{t_{\gamma}^* \partial^2}{\partial x \partial t_{\gamma}^*} n_{\gamma}(T_{\text{C}}x, t_{\gamma}^*), \quad (\text{A10})$$

with

$$B_{x,\eta^*} = \sqrt{1 - \left( \frac{x_{\eta^*}}{x} \right)^2}; \quad x_{\eta^*} = \frac{m_{\pi^0}/T_{\text{C}}}{\tan^{-1}(e^{-\eta^*})}.$$

Assuming  $\bar{N}_{\gamma} = 2\bar{N}_{\pi^0}$ , and substituting the explicit form of  $n_{\gamma}(E_{\pi^0}^*, t_{\gamma}^*)$  given by Eq. (11) into Eq. (A10) with  $E_{\pi^0}^* = T_{\text{C}}x$ , finally we obtain the kinematical relation between  $\gamma$  and  $\pi^0$  pseudo-rapidity distributions

$$2 \frac{dN_{\pi^0}}{d\eta^*} = \left[ 1 + \frac{1}{2} \left( \frac{m_{\pi^0}}{p_0} \right)^2 \frac{\Delta(\eta^*)}{F_0(\tau_{\eta^*})} \tanh^2 \eta^* \right] \frac{dN_{\gamma}}{d\eta^*}, \quad (\text{A11})$$

with

$$\begin{aligned} \Delta(\eta^*) &= \int_{x_{\eta^*}}^1 \frac{dx}{x} \left( \ln \frac{1+B_{x,\eta^*}}{1-B_{x,\eta^*}} - B_{x,\eta^*} \right) (1-x)^4 e^{-\tau_{\eta^*}^* x} \\ &\times \left\{ \left( \frac{4/\tau_{\eta^*}^*}{1-x} + 1 \right) \left( x + \frac{\zeta}{1+\zeta\tau_{\eta^*}^*} \right) - \frac{1}{\tau_{\eta^*}^*} \right\}, \end{aligned} \quad (\text{A12})$$

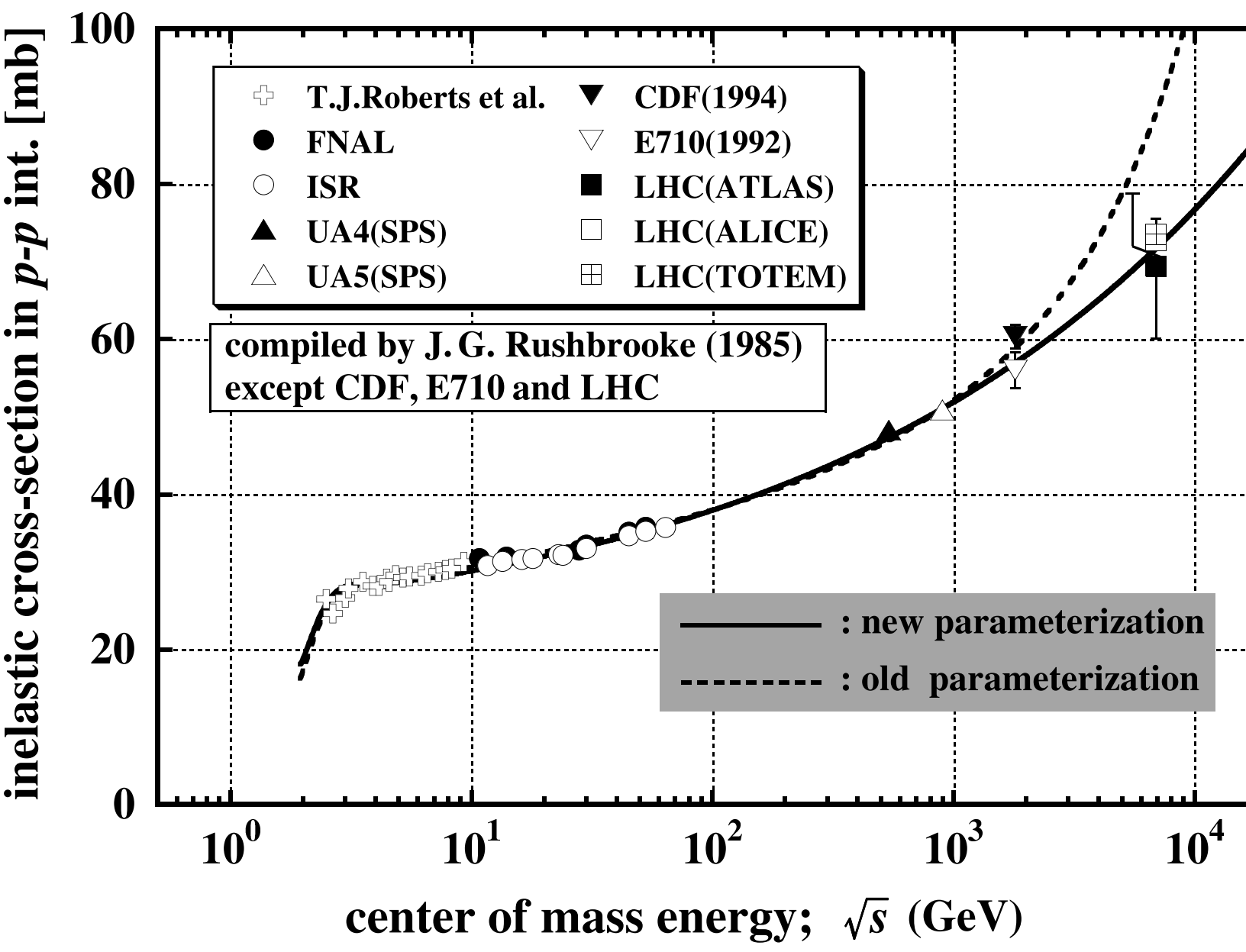
see Eq. (19) for  $\tau_{\eta^*}^*$ . In Fig. (19), we present the numerical value of the correction rate for the Sternheimer approximation with  $\alpha^* \approx 0$ , corresponding to the second term in the square bracket in Eq. (A11), where we assume  $p_0 = 200$  MeV/c, corresponding to approximately  $\bar{p}_{\text{T}} = 185, 189, 191, 193$  MeV/c for  $\sqrt{s} = 0.1, 0.2, 0.5, 1.0$  TeV respectively. We find that it is as large as 7% around  $\eta^* \approx 2$  at  $\sqrt{s} = 1$  TeV.

## References

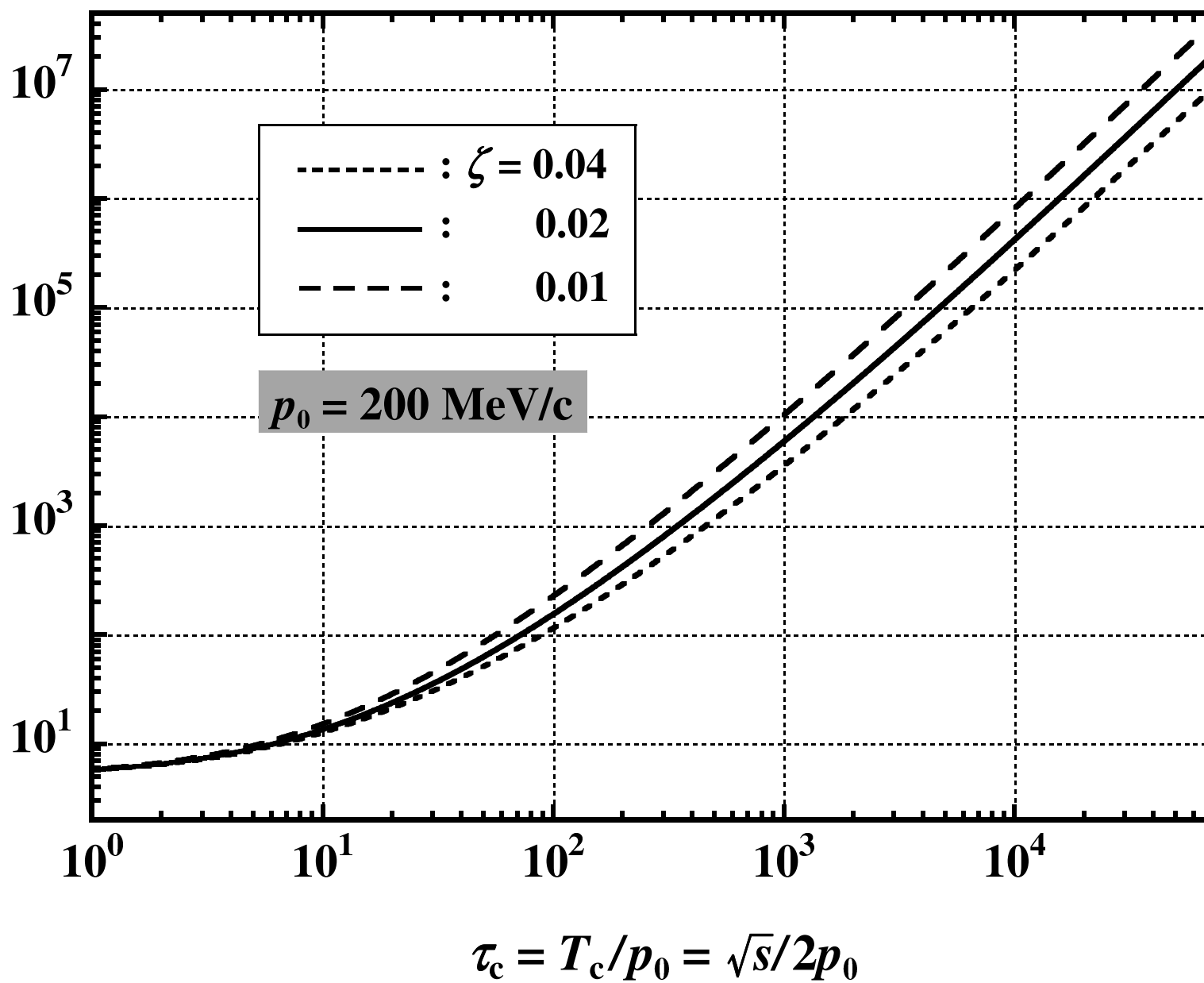
- [1] R. Suzuki, J. Watanabe, T. Shibata, *Astropart. Phys.* **23** (2005) 510.
- [2] F.A. Aharonian, J. Buckley, T. Kifune, G. Sinnis, *Reports on Prog. in Phys.* **71** (2008) 096901.
- [3] F.W. Stecker, *Astrophys. J.* **185** (1973) 499.

- [4] O. Adriani et al. (LHCf Collab.), *Phys. Lett. B* 703 (2011) 128.
- [5] G. Aad et al. (ATLAS Collab.), arXiv:1104.0326 (2011).
- [6] H. Aizu et al., *Suppl. Prog. Theor. Phys.* 16 (1960) 54.
- [7] P.J. Karol, *Phys. Rev. C* 11 (1994) 1203.
- [8] T. Shibata et al., *Astrophys. J.* 612 (2004), 238.
- [9] Rushbrooke, CERN-EP/85-178, November 1, 1985.
- [10] F. Abe et al., *Phys. Rev. D* 50 (1994) 5550.
- [11] N.A. Amos et al., *Phys. Lett. B* 243 (1992) 158.
- [12] C.M.G. Lattes et al., *Suppl. Prog. Theor. Phys.* 47 (1971) 1.
- [13] S.J. Brodsky, G. Farrar, *Phys. Rev. Lett.* 31 (1973) 1153;  
D. Sivers, S.J. Brodsky, R. Blankenbecler, *Phys. Reports* 23 (1976).
- [14] D.V. Bugg et al., *Phys. Rev. B* 133 (1964) 1017.
- [15] M. Fidecaro et al., *Nuovo Cim.* 24 (1962) 73.
- [16] K. Jaeger et al., *Phys. Rev. D* 11 (1975) 1757.
- [17] K. Jaeger et al., *Phys. Rev. D* 11 (1975) 2405.
- [18] A. Shenger et al., *Phys. Rev. D* 11 (1975) 1733.
- [19] G. Neuhofer et al., *Phys. Lett. B* 38 (1972) 51.
- [20] M.B.C. Santos et al., ICR-Report-91-81-7, ICRR, Univ. of Tokyo, July 1, 1981.
- [21] J.G. Alner et al., *Nucl. Phys. B*291 (1987) 261;  
J.G. Alner et al., *Phys. Rep.* 154 (1987) 5&6 247.
- [22] Y. Yamamoto et al., in: *Proceedings of the 21st ICRC, O.G.6.2, 1990*, p. 146.
- [23] M.G. Poghosyan et al. (ALICE Collaboration), arXiv:1109.4510v1 [hep-ex] 21 Sep 2011.
- [24] G. Latino et al. (TOTEM Collaboration), arXiv:1110.1008v1 [hep-ex] 5 Oct 2011.
- [25] E. Konishi et al., *Prog. Theor. Phys.* 56 (1976) 1845.
- [26] T. Shibata, N. Honda, J. Watanabe, *Astropart. Phys.* 27 (2007) 411.
- [27] T. Shibata, T. Ishikawa, S. Sekiguchi, *Astrophys. J.* 727 (2011), 38.

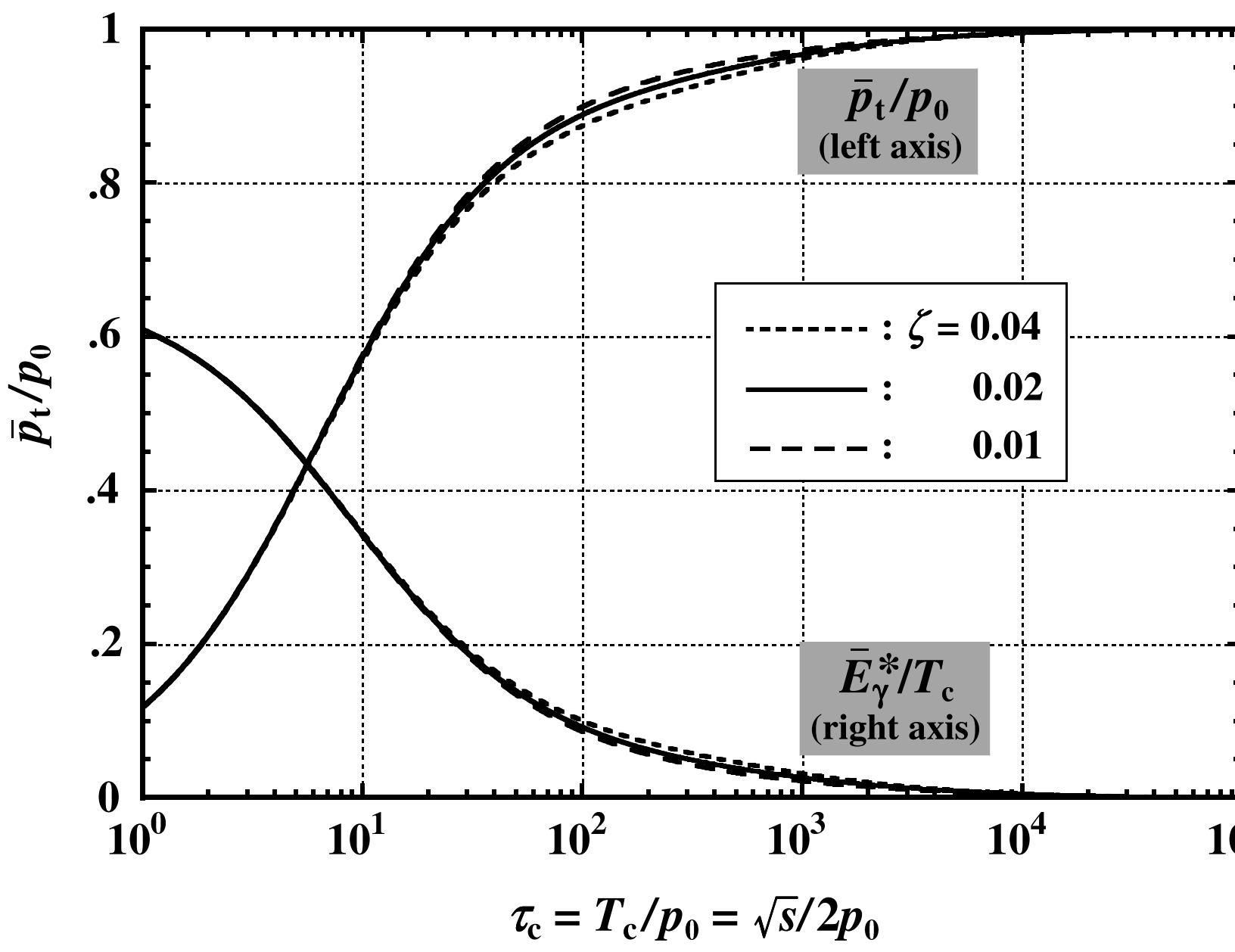
- [28] The CTA Consortium, arXiv:1008.3703 (2010).
- [29] N.N. Kalmykov, S.S. Ostapchenko, *Yad. Fiz.* 56 (1993) 105;  
N.N. Kalmykov, S.S. Ostapchenko, *Phys. At. Nucl.* 56 (1993) 346.
- [30] B. Peters, *Suppl. Nuovo Cim.* 14 (1959) 436.
- [31] H. Sato, Master Thesis (Aoyama-Gakuin University, 2011).
- [32] R.M. Sternheimer, *Phys. Rev.* 99 (1955) 277.
- [33] C.M.G. Lattes et al., *Suppl. Prog. Theor. Phys.* 47 (1971) 1.
- [34] T.K. Gaisser, R.K. Shafer, *Astrophys. J.* 394 (1992) 174.
- [35] G. Cavallo, R.J. Gould, *Nuovo Cimento B* 2 (1971) 77.
- [36] S.A. Stephens, G.D. Badhwar, *Astrophys. & Space Sci.* 76 (1981) 213.
- [37] J.G. Rushbrooke, CERN-EP/84-34, March 19, 1984.

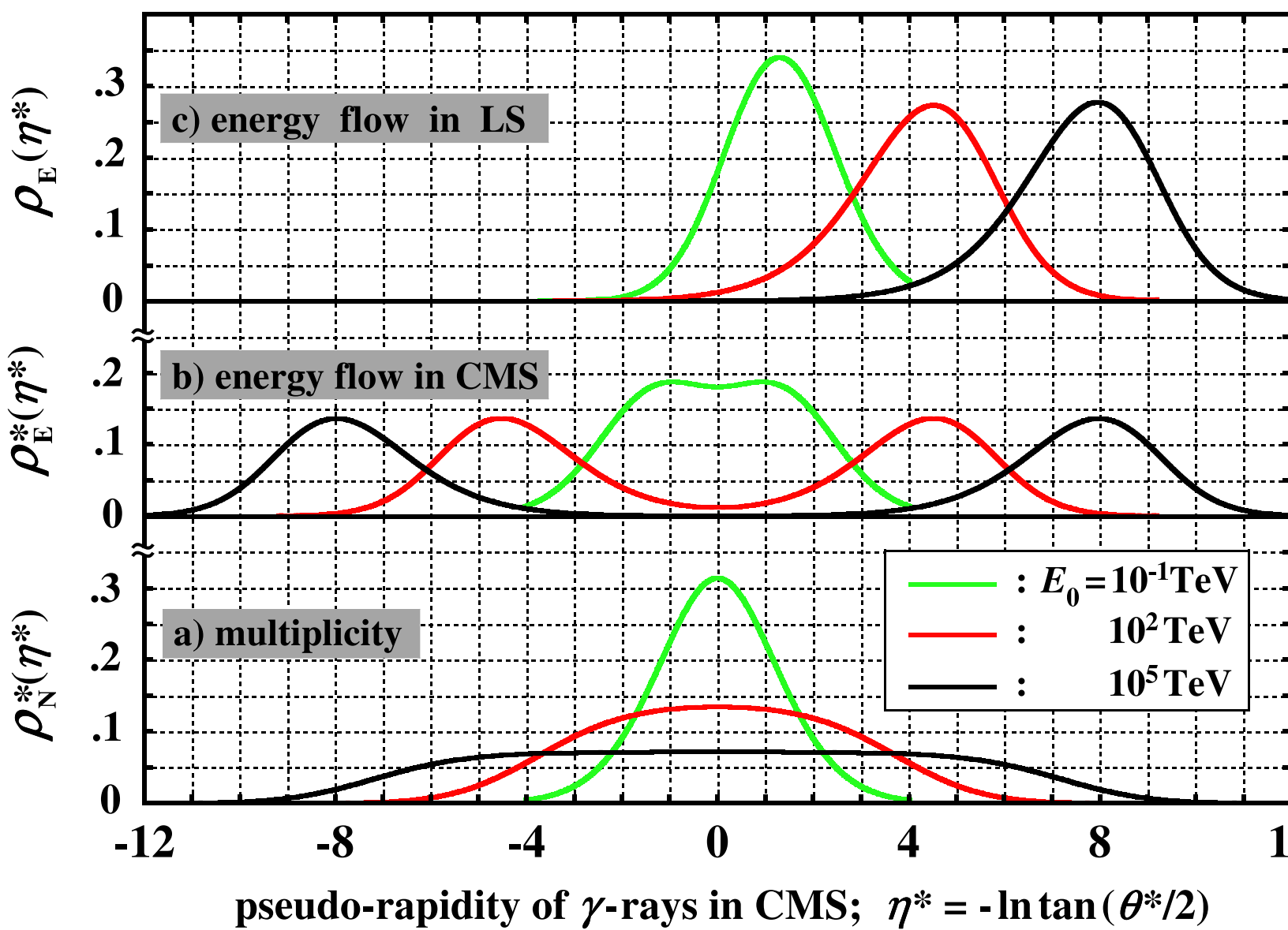


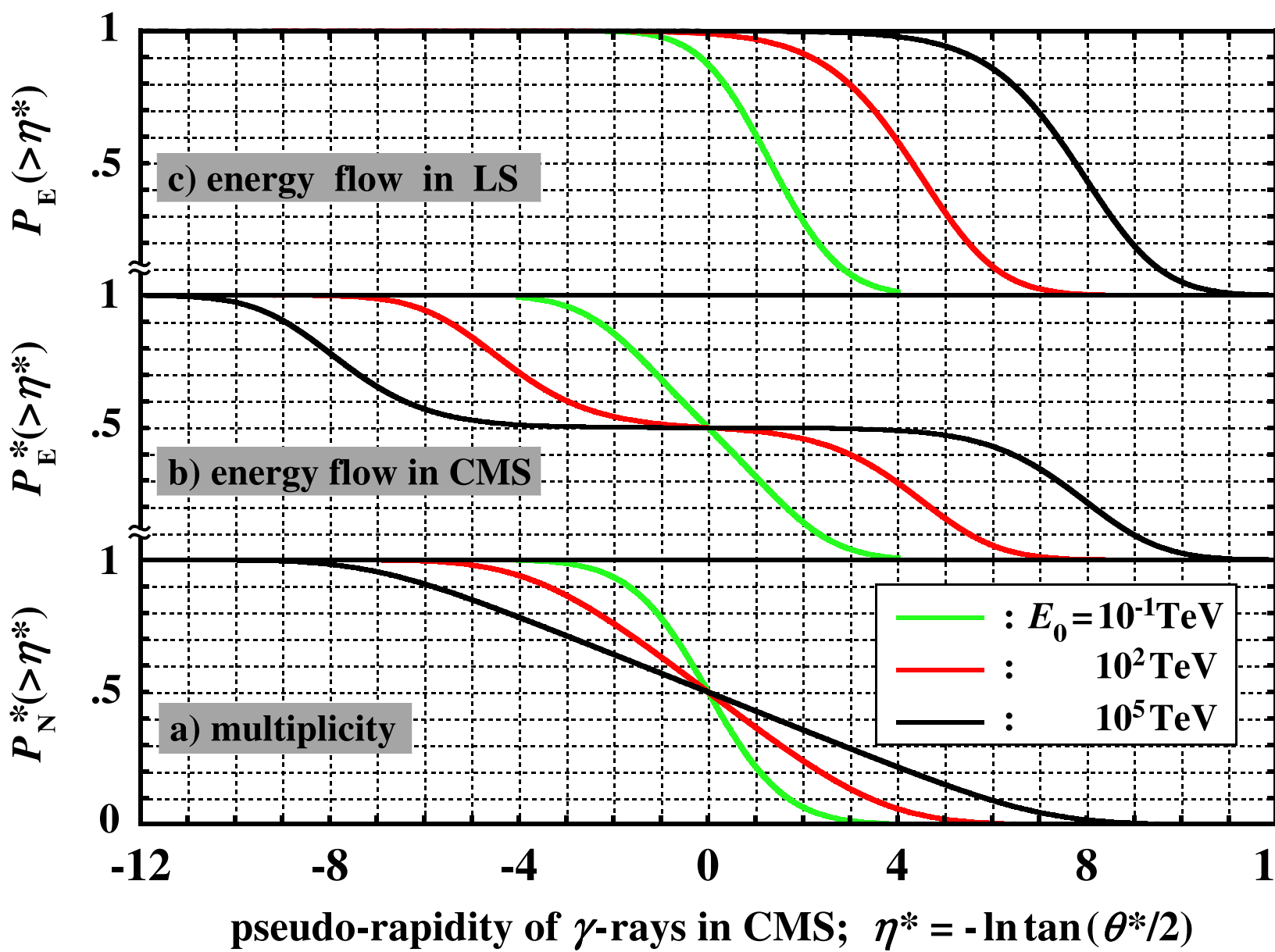
normalization constant;  $\Theta_c$

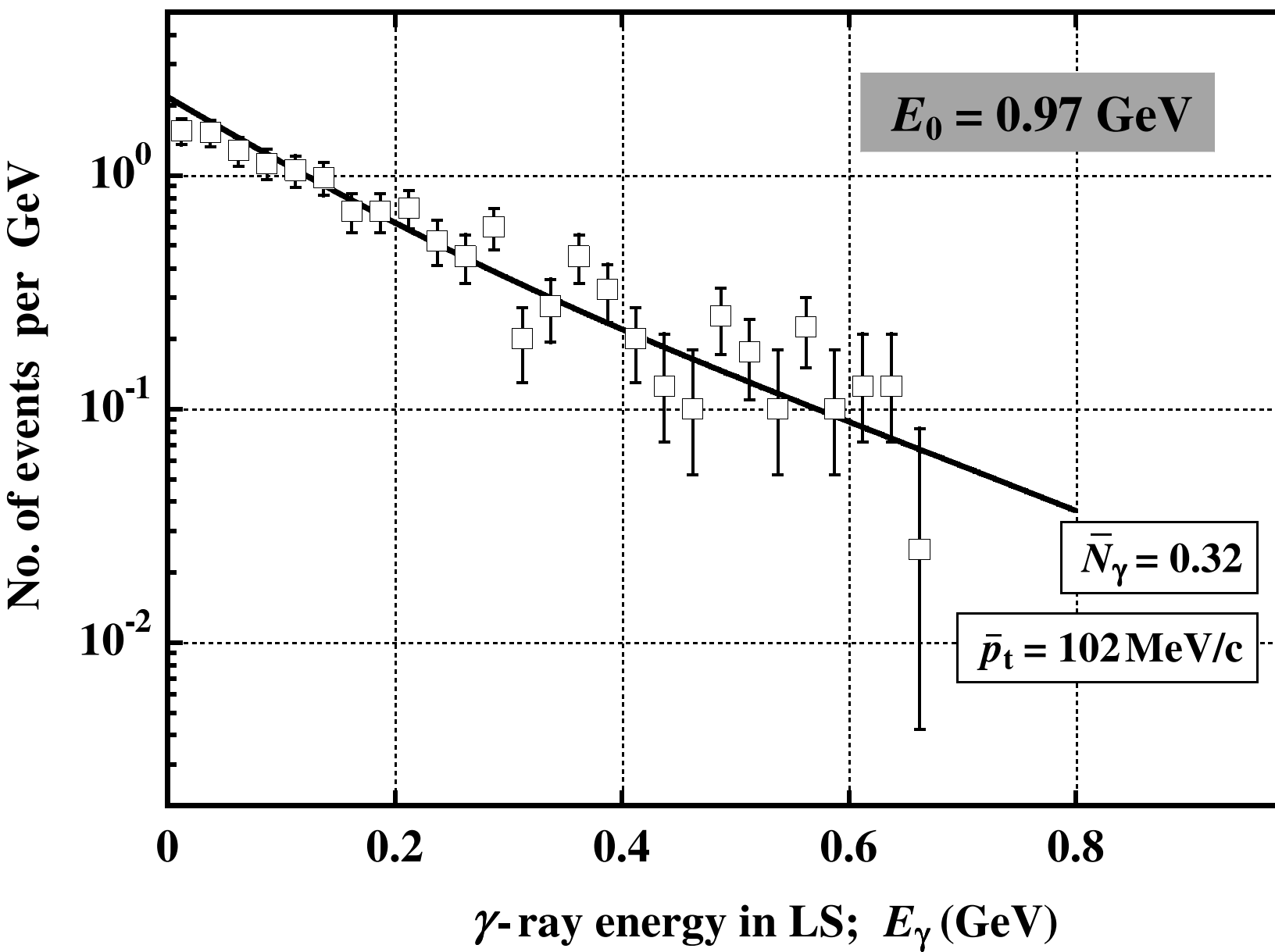


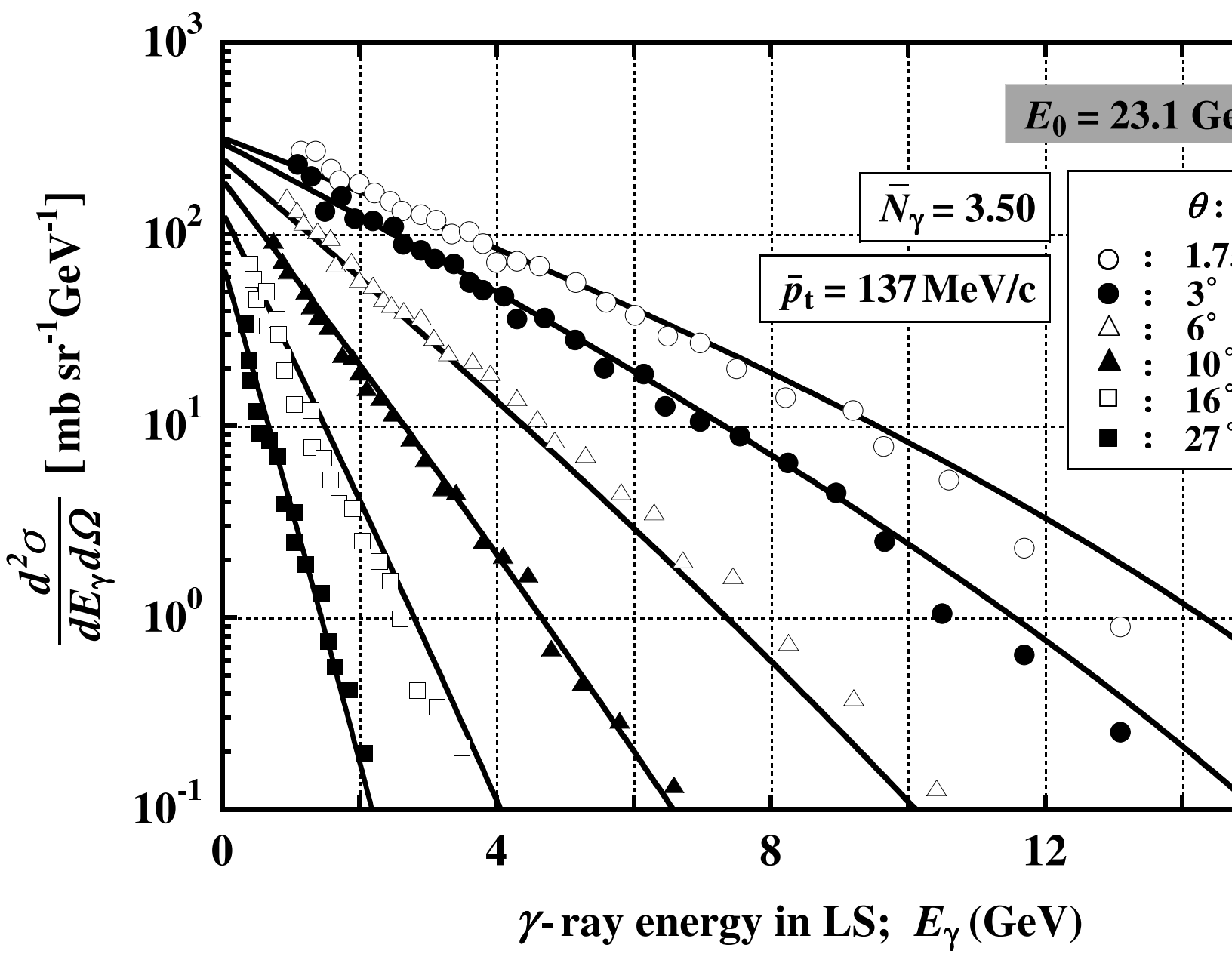


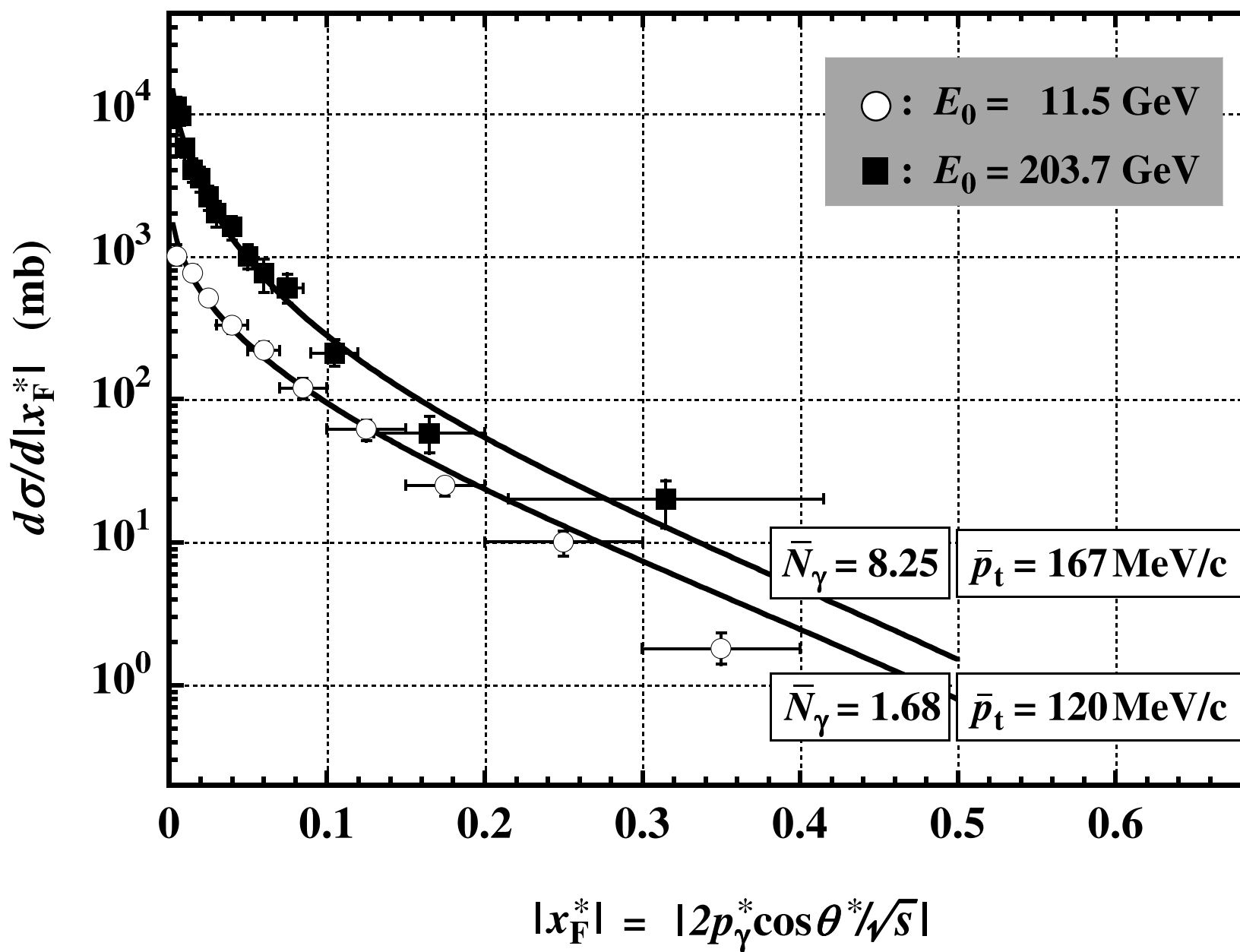


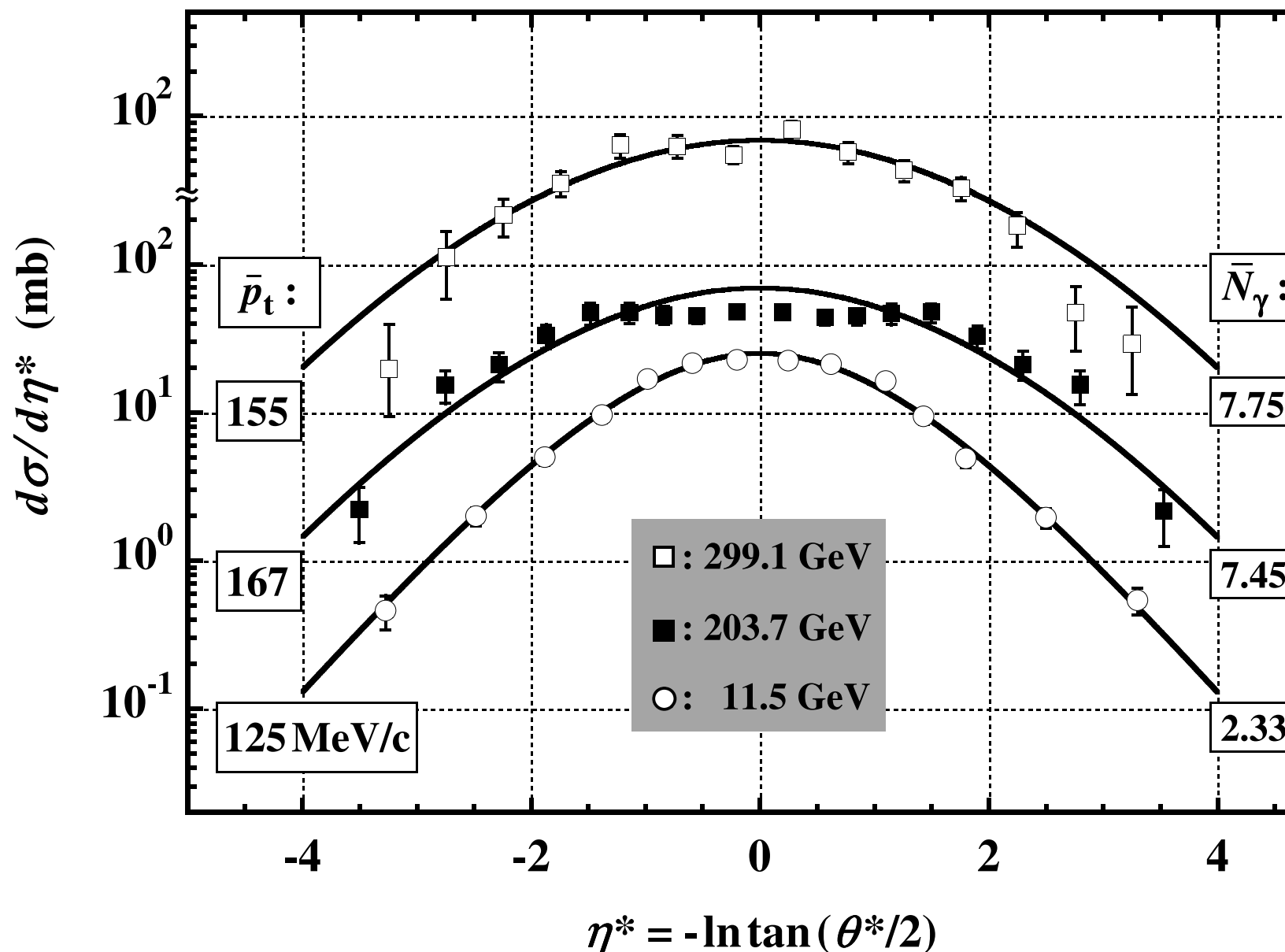


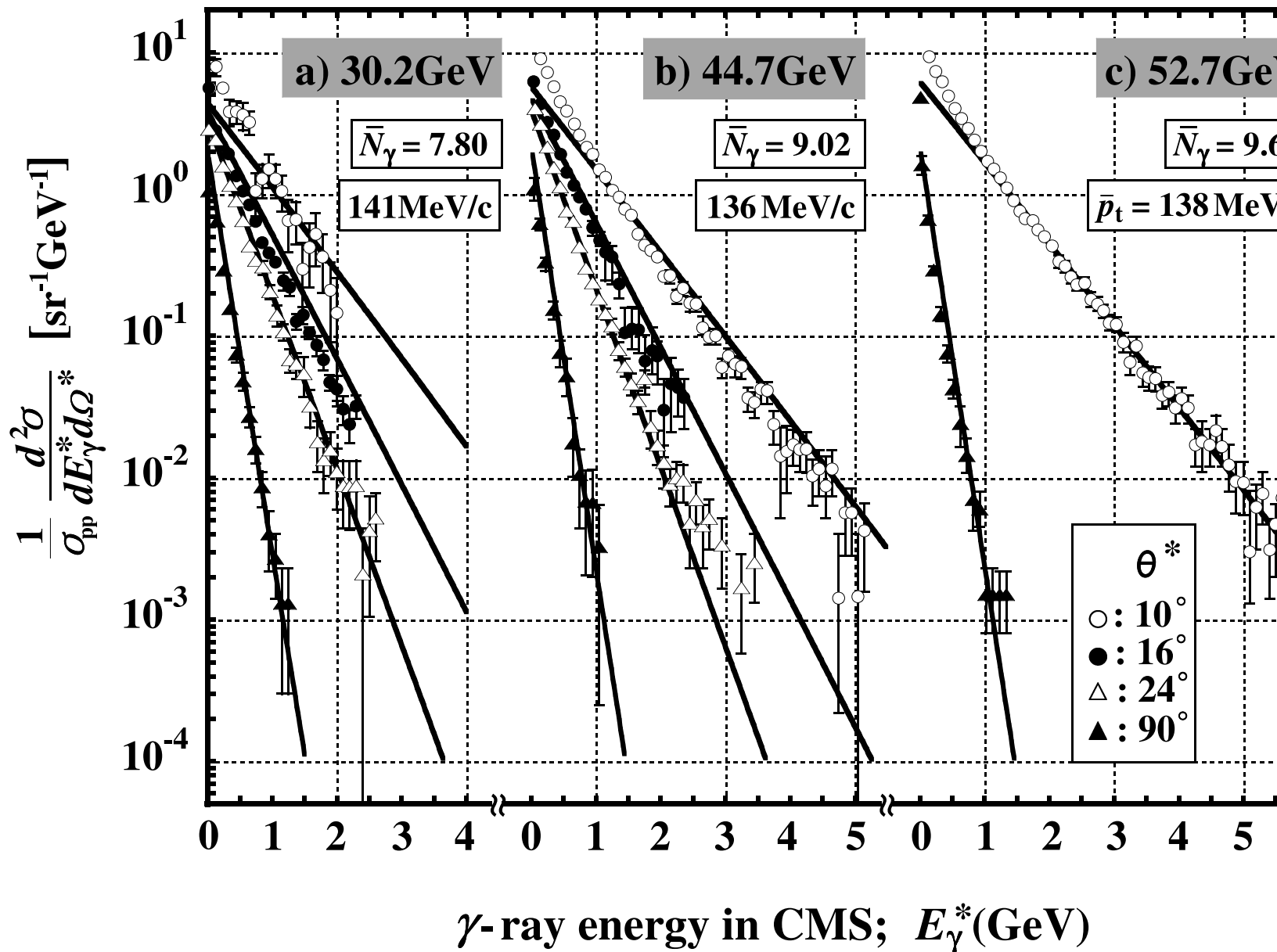




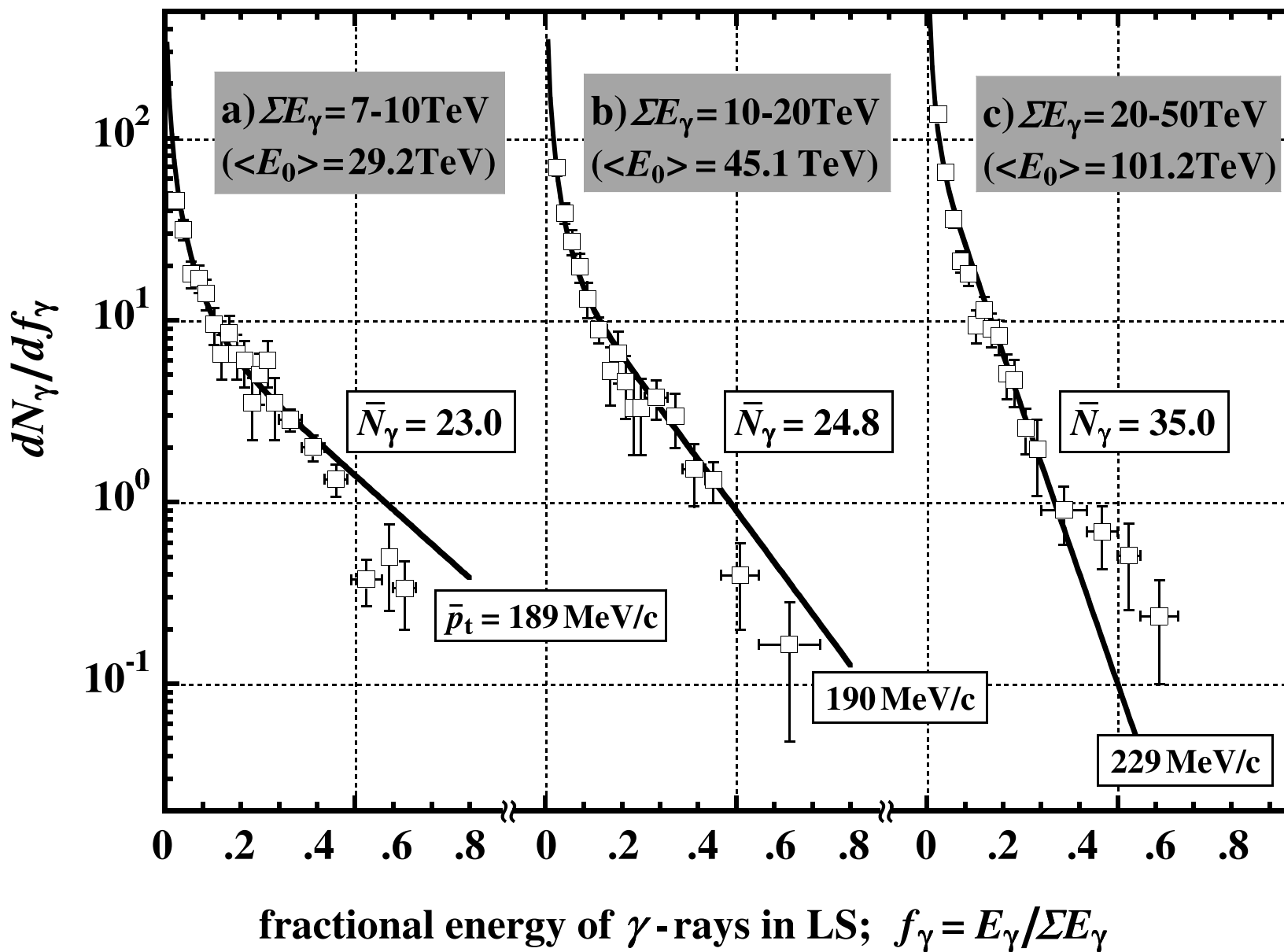


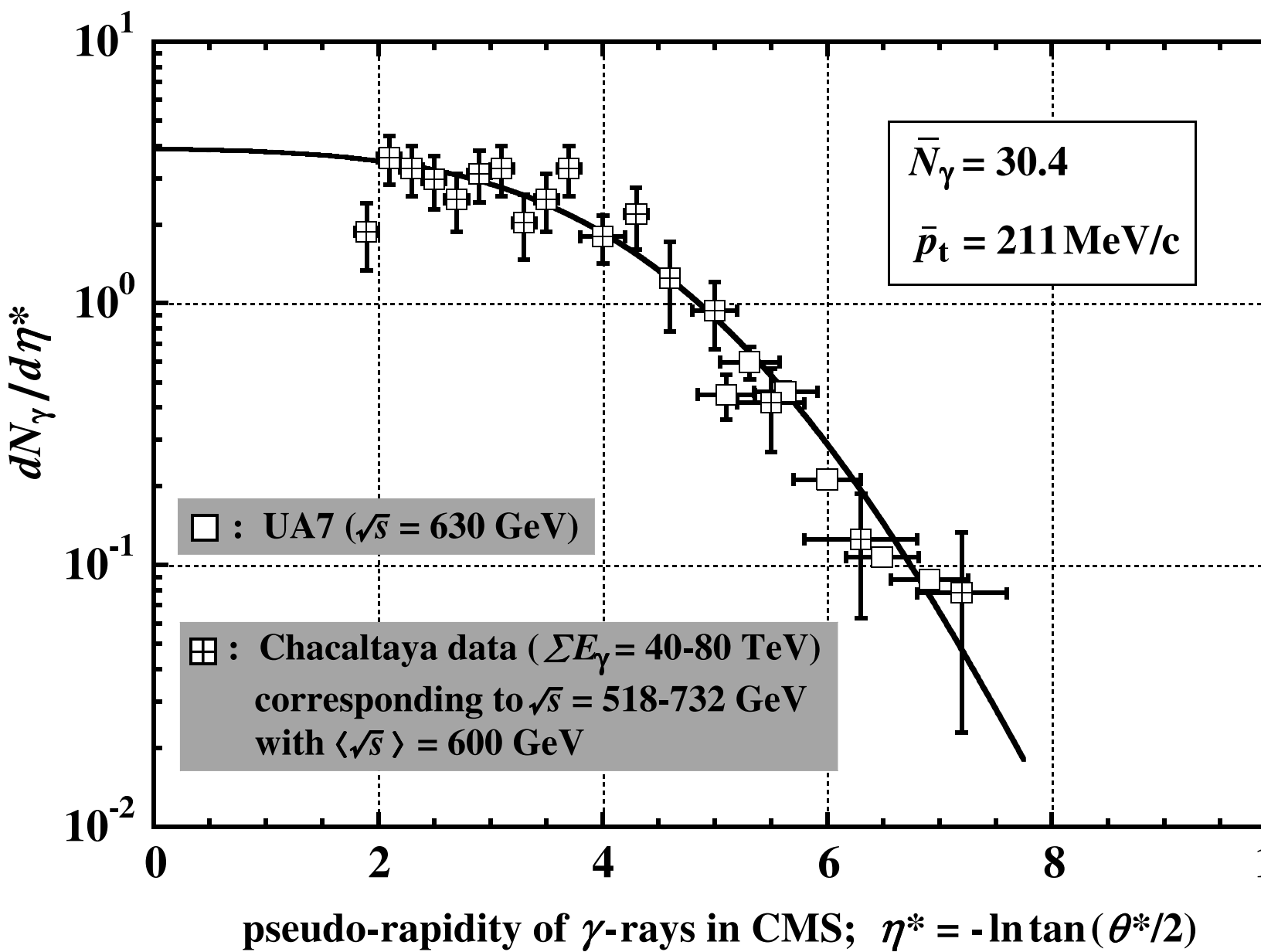


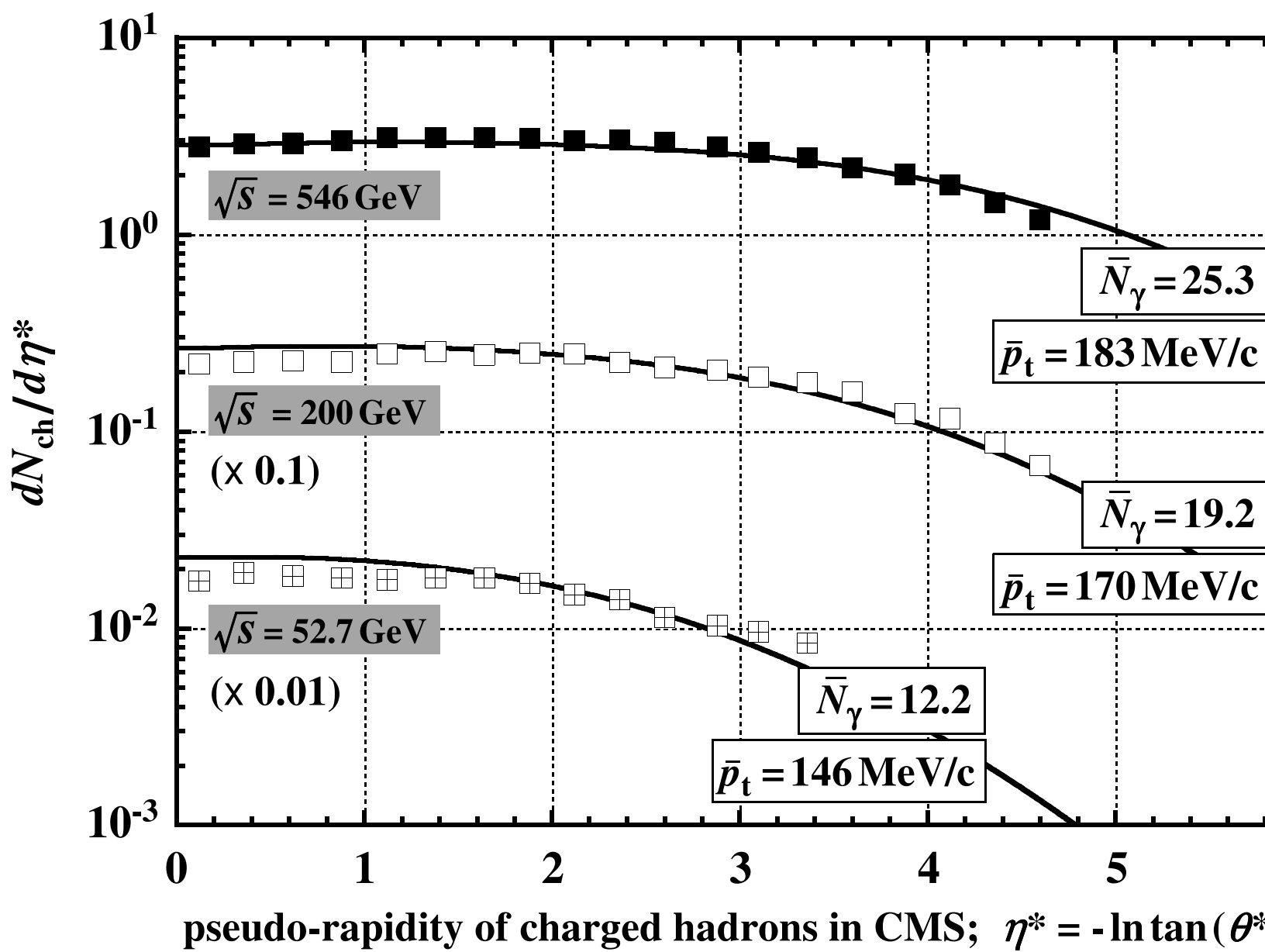


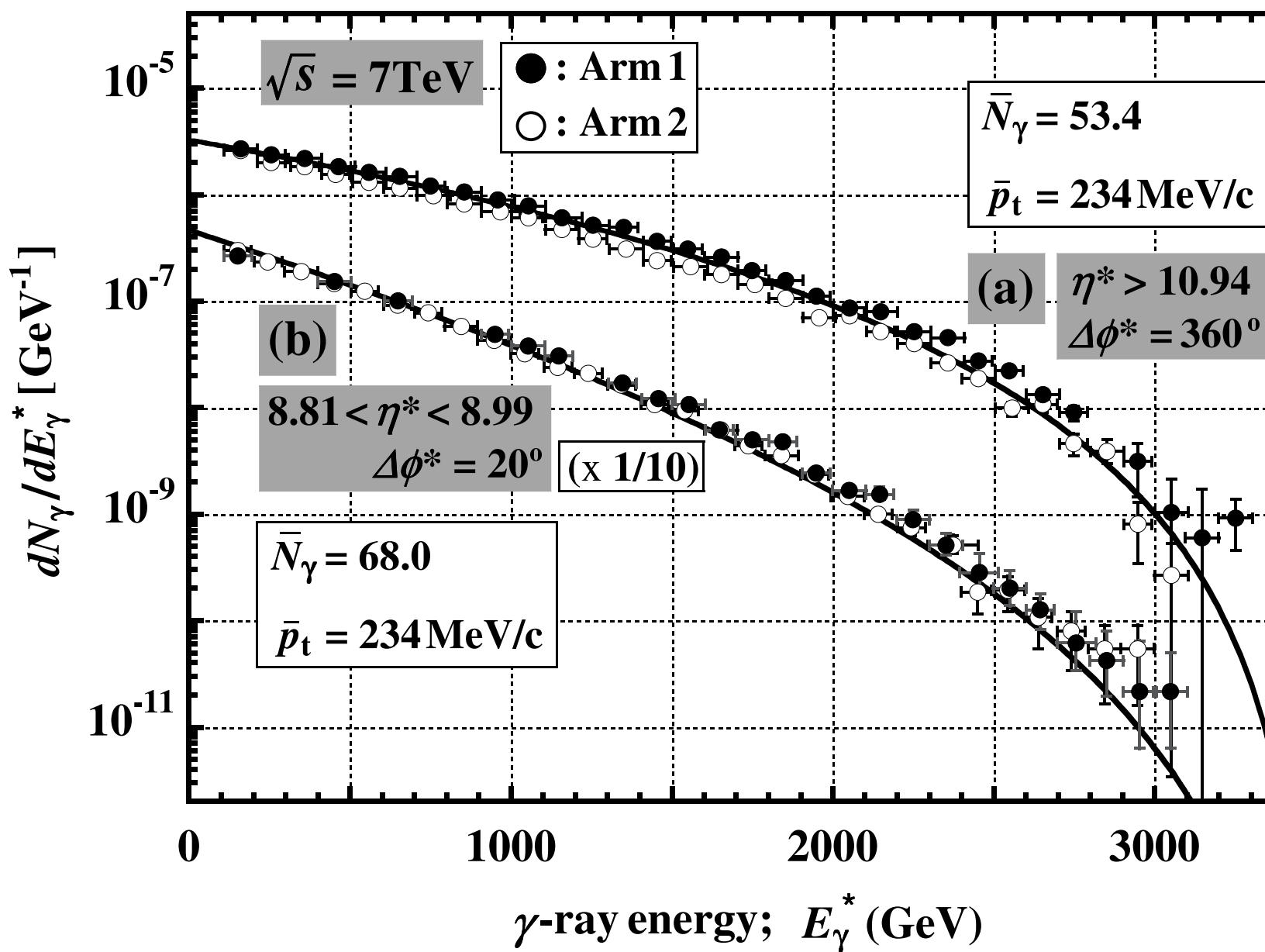


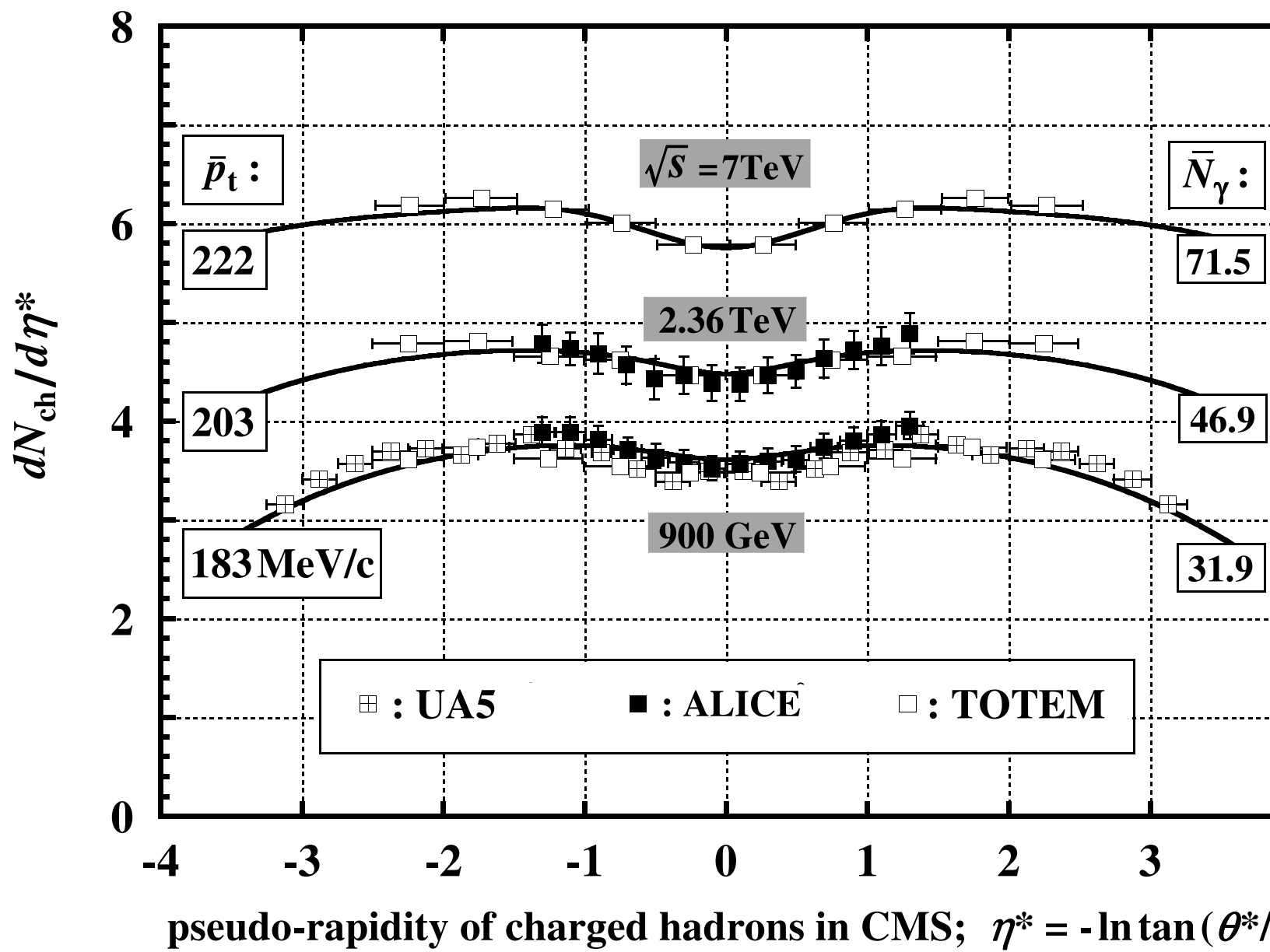






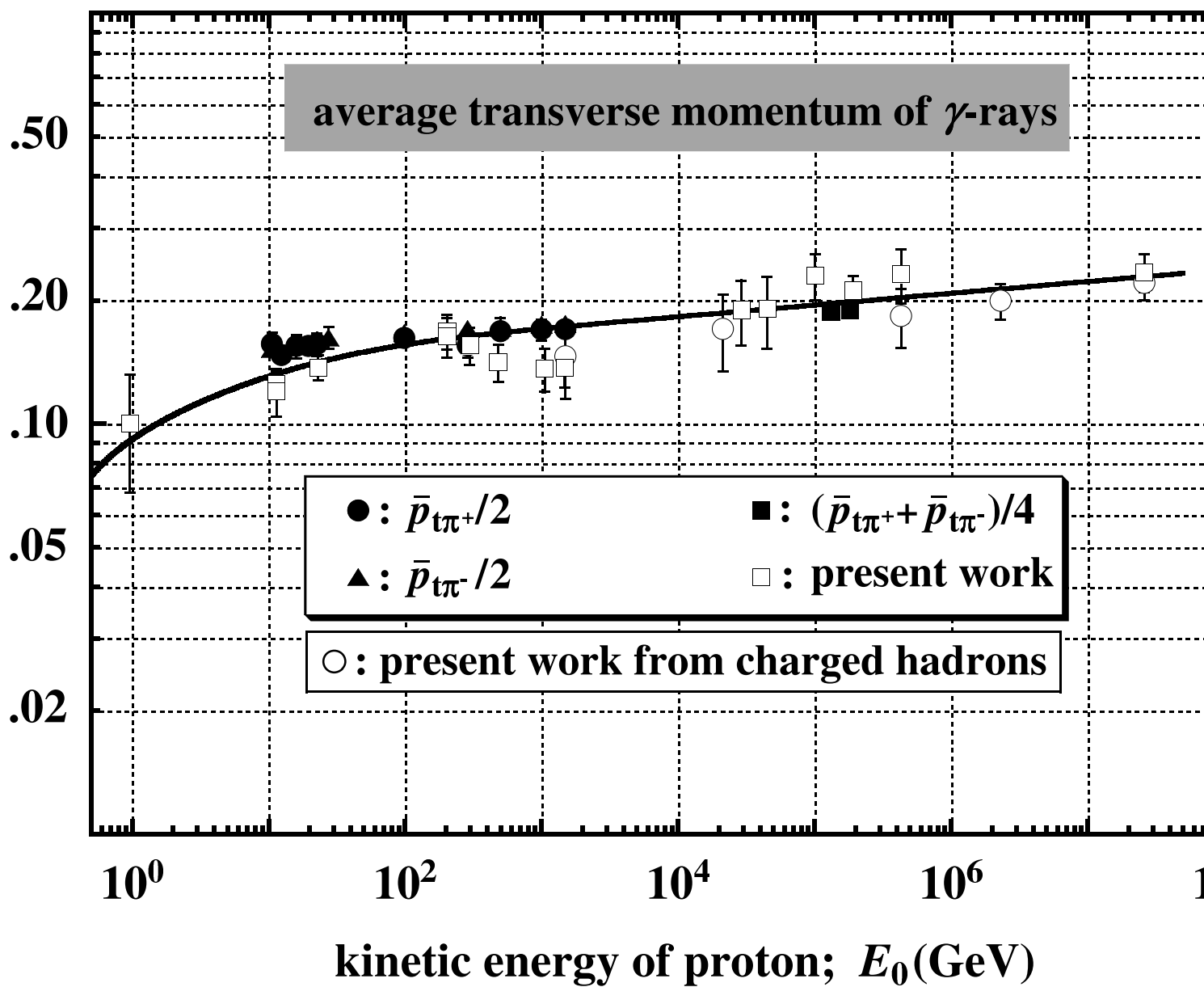




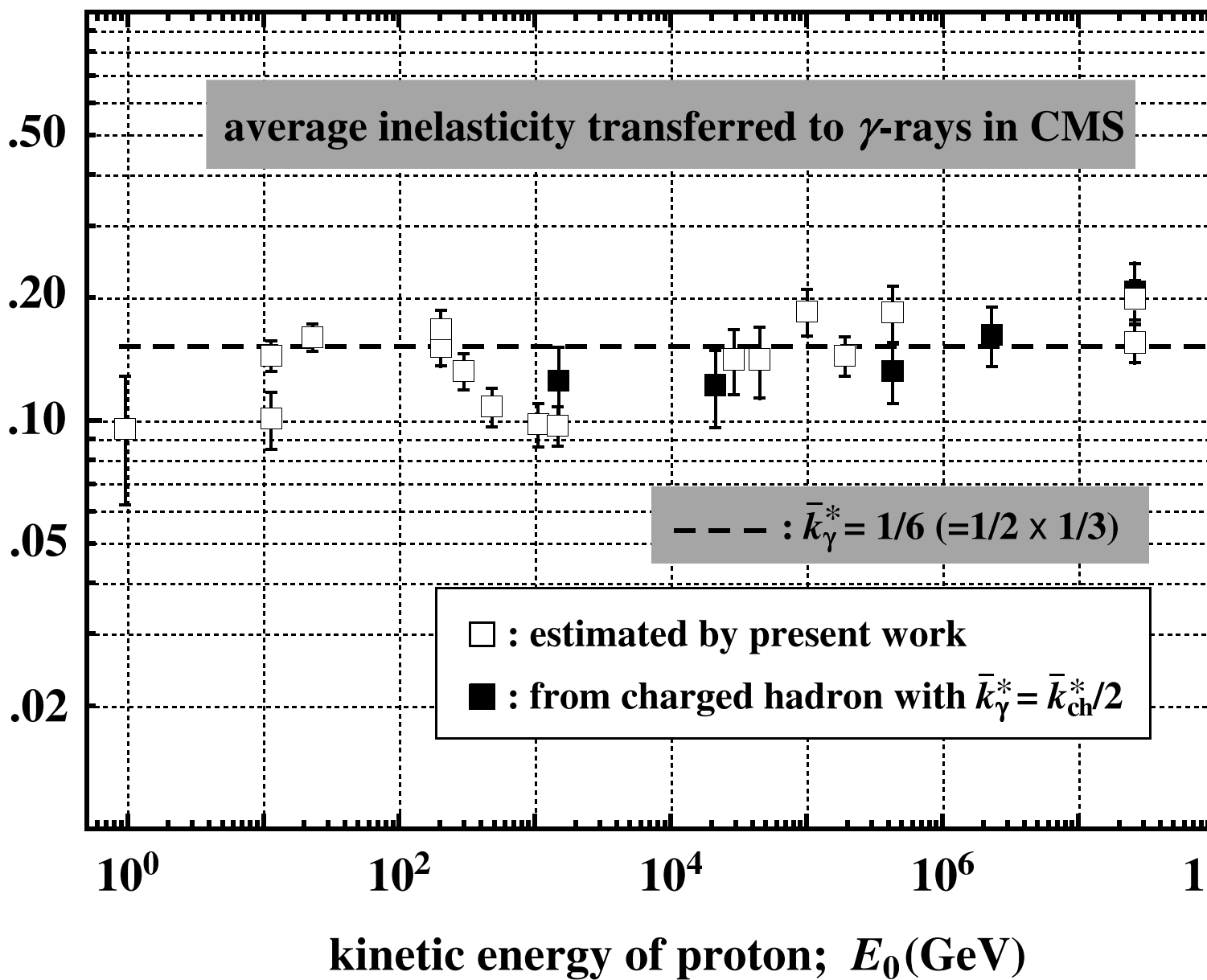




transverse momentum;  $\bar{p}_t$  (GeV/c)

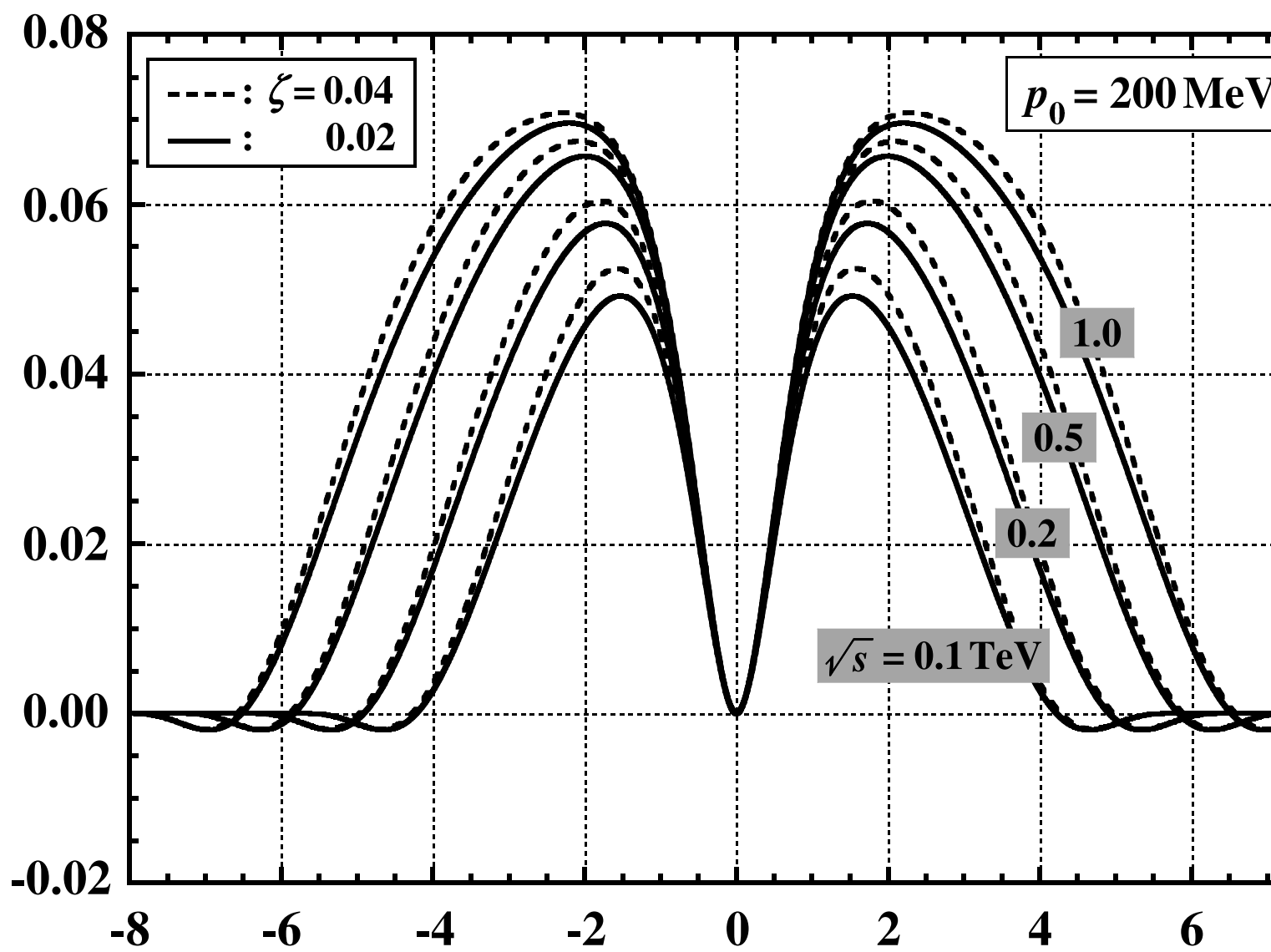


inelasticity transferred to  $\gamma$ 's;  $\bar{k}_\gamma^*$





correction rate for Sternheimer approx.



pseudo-rapidity of charged hadrons in CMS;  $\eta^* = -\ln \tan(\theta/2)$